Sex-specific Dominance and Its Effects on Allelic Diversity in Sexually Antagonistic Loci

Mattias Siljestam[1*] , **Claus Rueffler** [1†], **and Göran Arnqvist** [1†]

[1]Department of Ecology and Genetics, Animal Ecology, Uppsala University, Norbyvägen 18D, 752 36 Uppsala, Sweden
[*]To whom correspondence should be addressed. E-mail: m@siljestam.com
[†]These authors share senior authorship
ORCIDs: Siljestam, https://orcid.org/0000-0002-3720-4926; Rueffler, https://orcid.org/0000-0001-9836-2752; Arnqvist, https://orcid.org/0000-0002-3501-3376

Sexually antagonistic (SA) selection, favouring different alleles in males and females, can contribute to the maintenance of genetic diversity. While current theory predicts that biallelic polymorphism can be maintained in SA loci, particularly with strong selection or sex-specific dominance, some candidate SA loci harbour more than two segregating alleles. This highlights a gap in our understanding of the origin and maintenance of SA genetic variation. We present a mathematical model to explore the evolution of alleles at either an autosomal or an X-linked locus under SA selection, affecting a quantitative trait with distinct female and male optima. We show that additive allelic effects predict only biallelic polymorphism, and only under symmetric and relatively strong selection. Polyallelic polymorphism can evolve under conditions of sex-specific or X-linked dominance for the trait, particularly under weak selection, such that several alleles coexist in a single population through balancing selection. Our analysis furthermore shows that sex-specific dominance (and X-linked dominance) evolves when permitted, thus promoting the evolution of polyallelic polymorphism. We conclude that SA selection can drive the co-evolution of sex-specific dominance and polyallelic polymorphism, particularly under weak selection, which reduces the gender load. To assess these findings, we analyse segregating variation in three populations of a seed beetle model system and find support for our predictions: (i) candidate SA loci show a relatively strong signal of polyallelic polymorphism and (ii) loci with the strongest signal of polyallelic polymorphism are enriched with genes associated with known SA phenotypes.

sexual conflict | genetic polymorphism | heterozygote advantage | dominance reversal | Bruchinae

Introduction

Our understanding of the maintenance of genetic variation in loci and traits under selection is still incomplete, and the relative roles of mutation-selection balance, balancing selection and other processes remains debated. Quantitative assessments suggest that some form of balancing selection must contribute to the maintenance of polymorphisms for fitness-related traits (Charlesworth and Hughes, 2000; Mitchell-Olds et al., 2007; Charlesworth, 2015). Perhaps the most general generator of balancing selection are trade-offs resulting in antagonistic pleiotropy, whereby alternative alleles are favoured by selection in different contexts (e.g., environmental conditions, ontogenetic stages, age classes or sexes). Previous theory suggests that the conditions under which antagonistic pleiotropy maintains biallelic polymorphism (BAP) at SA loci may be quite restricted (Prout, 2000), requiring symmetric and strong selection (e.g., Kidwell et al., 1977; Flintham et al., 2023), disassortative mating by genotype (Arnqvist, 2011), dominance under sex-linkage (Rice, 1984; Patten and Haig, 2009) or dominance reversal (Kidwell et al., 1977; Fry, 2010). Dominance reversal, where each allele shows dominance in the context in which it is beneficial and recessivity when it is disfavoured, has a particularly high potential capacity to promote the maintenance of genetic variation (Kidwell et al., 1977; Wilder et al., 2016; Wittmann et al., 2017; Grieshop and Arnqvist, 2018; Connallon and Chenoweth, 2019; Grieshop et al., 2024).

Dominance reversal has by tradition been considered unlikely, partly based on the observation that mutations with major effects (e.g., causing disorders in humans) tend to be unconditionally dominant or recessive (Curtsinger et al., 1994). Although our understanding of the proximate

mechanisms of dominance is still limited (Huber et al., 2018), both theory (Otto and Bourguet, 1999; Spencer and Priest, 2016) and data (Billiard and Castric, 2011) suggest that dominance relationships can and do evolve (Grieshop et al., 2024). Moreover, a few recent studies are consistent with wide-spread dominance reversal, for example, across the sexes (Meiklejohn et al., 2014; Barson et al., 2015; Grieshop and Arnqvist, 2018; Mérot et al., 2020) and thermal environments (Chen et al., 2015).

Sexually antagonistic (SA) selection is a potentially near ubiquitous generator of antagonistic pleiotropy in taxa with separate sexes, due to the fact that two distinct and persistent genetic environments (males and females) exist in typically stable and equal proportions. Here, explicit genetic modelling has shown that sex-specific dominance is a predicted outcome in SA loci (Fry, 2010; Spencer and Priest, 2016; Connallon and Chenoweth, 2019) and a few empirical studies have confirmed that SA alleles beneficial in one sex indeed tend to be dominant in that sex but recessive in the other (Barson et al., 2015; Grieshop and Arnqvist, 2018; Pearse et al., 2019; Glaser-Schmitt et al., 2021). A notable and intriguing property of several putative SA loci is the apparent segregation of more than two loci. Polyallelic polymorphism (PAP) has, for example, been documented for the VGLL3 locus in salmon (Barson et al., 2015), the Cyp6g1 locus in *Drosophila melanogaster* (Schmidt et al., 2010; Hawkes et al., 2016), several seminal fluid protein genes in *Drosophila* (Wagstaff and Begun, 2005) and neurogenetic loci in voles (Lonn et al., 2017). The maintenance of PAP in loci under selection is generally not well understood (Lewontin et al., 1978; Spencer and Mitchell, 2016), and the presence of PAP in candidate SA loci suggests that additional theoretical work would be helpful. We note that sexual conflict mediated by the compatibility between a pair of interacting loci with sex-limited expression (i.e., interlocus sexual conflict; Arnqvist and Rowe, 2005) can act to maintain PAP through specific pairwise compatibility between for example male ligands and female receptors (Gavrilets and Waxman, 2002; Haygood, 2004), but this may not be directly applicable to SA loci.

In this study, our aim is three-fold. First, we assess under which conditions we should expect the emergence of BAB or PAP through gradual evolution acting on locus coding for a quantitative trait under SA selection, and whether sex-specific dominance is an emergent phenomenon in loci showing SA polymorphism. Unlike previous modelling efforts, we evaluate the effects of sex-specific dominance for trait expression rather than for fitness. Second, given that previous models of SA loci are restricted to biallelic scenarios, we ask whether the evolution of sex-specific dominance is associated with the origin and maintenance of PAP in SA loci. Third, we use population genomic data from three populations of an insect model system to ask whether loci more likely to show SA pleiotropy are also more likely to show PAP. We develop a general mathematical model that confirms that sex-specific dominance indeed evolves in loci showing SA polymorphism, and we find that this, in turn, generates PAP that acts to reduce segregation load. We get qualitatively similar results for dominance in X-linked loci. Our empirical data are consistent with an enrichment of PAP in candidate SA loci, such as X-liked loci and genes showing shared intermediate frequency polymorphism across populations, and genes showing the strongest signal of PAP were enriched with genes encoding known SA phenotypes.

Model

We present a mathematical model describing allelic evolution at an autosomal locus subject to sexually antagonistic (SA) selection. This locus encodes a quantitative trait, denoted as z, for which females and males have different optima. The trait z could represent any shared characteristic, such as morphology or a life-history trait.

The survival probability (or viability) w of an individual decreases according to a Gaussian function with increasing deviation of its phenotypic trait value z from the sex-specific optimum, as illustrated in Figure 1. We here choose, without loss of generality, that the phenotypic optimum for fe-

males is given by a lower value than that for males (as in Fig. 1). The width of the Gaussian functions ($\sigma_{♀}$ and $\sigma_{♂}$) relative to the distance δ between the phenotypic optima determines the sex-specific strength of selection. Large values of $\delta\sigma_{♀}^{-1}$ and $\delta\sigma_{♂}^{-1}$ correspond to strong selection (large distance or narrow Gaussian functions). For presentation purposes, we set $\delta = 1$ in all simulations and refer to $\sigma_{♀}^{-1}$ and $\sigma_{♂}^{-1}$ as strength of selection.

Each allele is characterized by an allelic value x, which influences an individual's phenotypic trait value z. Thus, z is a function of the allelic values of the two alleles x_i and x_j present at a locus: $z(x_i, x_j)$. For individuals homozygote for an allele x, the phenotype is equal to the allelic value, $z(x, x) = x$. For heterozygote individuals carrying allele x_i and x_j, the resulting phenotype z falls between x_i and x_j, with the precise value determined by the dominance relationship between the two alleles.

Modelling dominance between an arbitrary number of alleles $x_1, x_2, \ldots, x_n$ it is not trivial. In this study, we assume a dominance hierarchy (Billiard et al., 2021) as illustrated in Figure 2 (which visualizes Eq. A1 in Appendix 1). The dominance relationship between any two alleles is characterized by a dominance parameter d, where $d > 0$ indicates dominance of alleles with larger allelic values and $d < 0$ dominance of alleles with smaller allelic values. Note that d is not equivalent to the classical dominance coefficient h, which specifies the dominance relationship between two particular

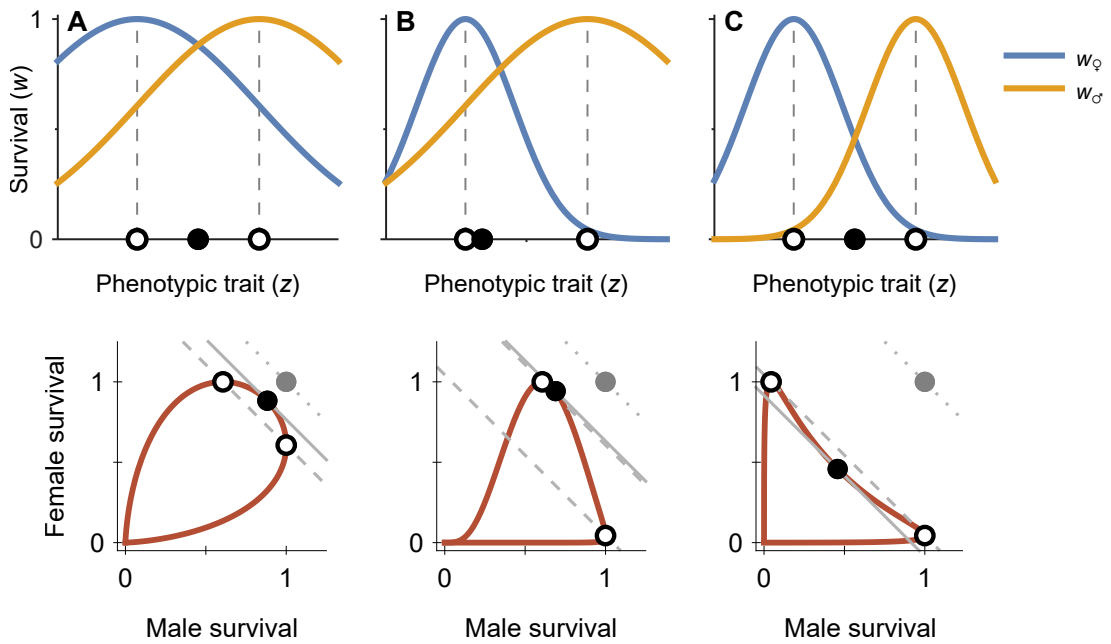

Figure 1. The upper panel shows sex-specific survival w as a function of the phenotypic trait z, and the lower panel illustrates the same Gaussian trade-offs, but with the two survivals shown as a parametric curve in z (cf. Levins, 1968, p. 16). Open dots indicate the phenotypic optima for females and males, while filled dots indicate the trait value that maximizes geometric mean viability across the two sexes. In the lower panel, contour lines of equal survival averaged across both sexes (marginal survival) are added in grey. Hatched lines indicate all combinations of female and male survival that have the same marginal survival as the phenotype that maximises survival in one sex. Solid lines do the same, but with the trait value maximizing mean geometric survival as reference. Finally, dotted lines pass through a filled grey dot that corresponds to the survival of individuals heterozygous for the two specialist alleles under full adaptive dominance. Since under sex-specific dominance females and males express different trait values, these dots do no longer lie on the parametric curve. In **A**, both sexes are under weak selection ($\sigma_{♀}^{-1} = 1 = \sigma_{♂}^{-1}$), while in **B** females are under strong selection while males are under weak selection ($\sigma_{♀}^{-1} = 2.5$, $\sigma_{♂}^{-1} = 1$). In **C**, both sexes are under strong selection ($\sigma_{♀}^{-1} = 2.5 = \sigma_{♂}^{-1}$).

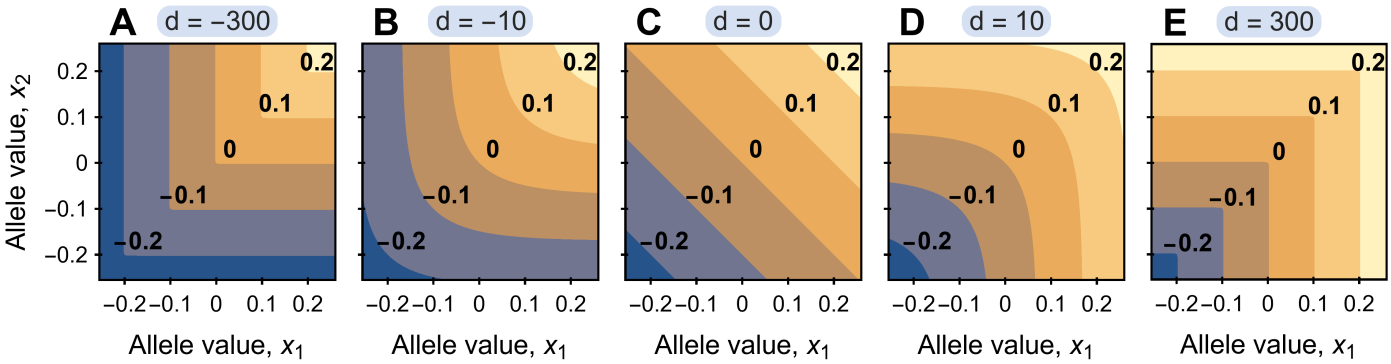

Figure 2. Contour plots of the phenotypic trait value z as a function of the two allelic values x_1 and x_2 at a locus under sexually antagonistic selection for different dominance parameters d (as determined by Eq. A1). **A** and **E** illustrate scenarios approximating full dominance of the allele with the smaller (**A**) or larger (**E**) x-value. These graphs result from a large negative d-value, approximating the min-function $z = \min(x_i, x_j)$ (corresponding to $h = 0$), and a large positive d-value, approximating the max-function $z = \max(x_i, x_j)$ (corresponding to $h = 1$), respectively. **C** shows additive allelic effects ($z = (x_i + x_j)/2$, or $h = 0.5$) as it results when the dominance parameter d is zero. Intermediate d-values, shown in **B** and **D**, lead to dominance patterns that depend on the magnitude of the difference between x_1 and x_2. Increasing differences result in close to full dominance, while additivity is approached for small differences (manifested as smooth corners along the diagonal in **B** and **D**, contrasting the sharp angles in **A** and **E**).

alleles. Instead, d determines the direction and degree of dominance for any pair of alleles. The parameter d can be related to h in certain scenarios. When $d = 0$ (as shown in Figure 2C), alleles act additively, corresponding to $h = 0.5$. For a large positive d (as depicted in Figure 2E), the allele with the larger allelic value is fully dominant, corresponding to $h = 1$. Conversely, for a large negative d (Figure 2A), the allele with the smaller allelic value is fully dominant, corresponding to $h = 0$.

In contrast to previous models of SA variation, thus, our model does not apply dominance to fitness (in our model given by survival w). Rather, dominance determines how allelic values x_i and x_j map onto the trait value z. Survival w is a consequence of z as described above. By allowing for different dominance parameters for females and males, $d_♀$ and $d_♂$, respectively, we introduce the possibility of sex-specific dominance, which occurs whenever $d_♀ \neq d_♂$. This is illustrated in Figure 3B-C.

Since classic theory predicts that the X-chromosome should be enriched with SA loci (Rice, 1984), consistent with some empirical data showing an important role for X-linked sites in sex-specific traits (Reinhold, 1998; Gibson et al., 2002; Dean and Mank, 2014; Ruzicka and Connallon, 2020), we also analyse a version of our model for X-linked loci. This version follows the same principles, with the exception that dominance can only be expressed by females, while a male that is hemizygous for x_i has a phenotype directly determined by its allelic value, $z = \delta x_i$. Consequently, dominance at an X-linked locus inherently exhibits sex-specific characteristics, and we demonstrate that the outcomes are qualitatively similar to those observed with sex-specific dominance at an autosomal locus.

Analyses. We use evolutionary invasion analysis to derive a condition for the emergence and maintenance of allelic diversity through repeated mutations in a locus coding for a quantitative trait under sexually antagonistic selection. Technically, this process is known as evolutionary branching (Metz et al., 1992; Geritz et al., 1998; Kisdi and

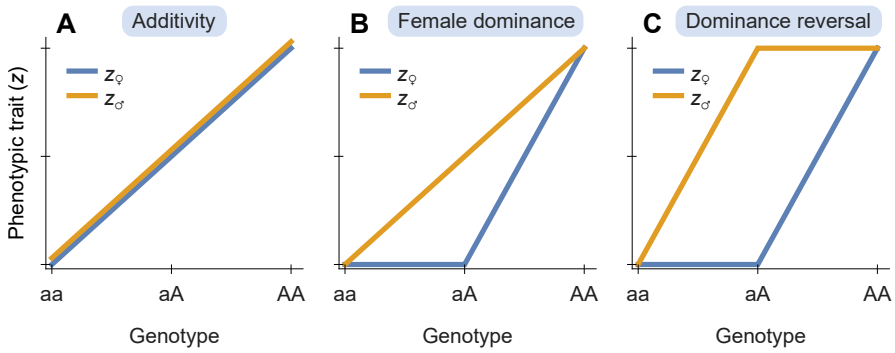

Figure 3. Phenotypic trait value resulting from two alleles, one favoured in females (x_a) and one in males (x_A). **A**. Additive allelic effects ($d_♀ = 0 = d_♂$, corresponding to $h = 0.5$). **B**. Sex-specific dominance with $d_♀$ large and negative and $d_♂ = 0$, corresponding to dominance in females ($h = 0$) and additivity in males ($h = 0.5$). **C**. Dominance reversal with $d_♀$ large and negative ($h = 0$) and $d_♂$ large and positive ($h = 1$).

Geritz, 1999; Doebeli, 2011). For details on the mathematical derivations, see Section S2 in the Supplementary Information. This method assumes a large population and rare mutations with small effects. We then use individual-based simulation that relax these assumptions to show that the analytical predictions are robust. Both our analysis and simulations use Wright-Fisher population dynamics with mutation and selection (Fisher, 1930; Wright, 1931).

Simulations. Our condition for the emergence of adaptive polymorphism predicts whether gradual evolution can result in two alleles that are subsequently maintained by balancing selection. We determine the robustness of our analytically derived condition and the final number of coexisting alleles with individual-based simulations.

Mutations are drawn from a normal distribution with an expected mutational step size of 0.02, where the sex-specific optima (see Figure 1) are positioned one unit apart. With a per-allele mutation probability of $\mu = 5 \times 10^{-7}$ and a population consisting of $N = 10^5$ individuals, new mutant alleles appear on average every tenth generation. This configuration is chosen as it ensures a low number of near-neutral alleles at mutation-drift equilibrium, allowing for alleles maintained through balancing selection to be identified, but not too low, ensuring sufficient mutation input for evolution to progress. To determine the number of coexisting alleles, we first bin alleles that are less than 0.02 units apart (≈ 1 mutation), and then count the minimum number observed in the population within the last 10% of a simulation run. This excludes most transient polymorphisms.

Simulations are initialized with a population monomorphic for an allelic value x drawn from an unimodal distribution with a mean corresponding to the trait value positioned exactly between the two optima. On the rare occasion that this initial x leads to an expected population size less than 50 for either sex, we redraw this x to avoid initial extinction. To ensure the number of coexisting alleles equilibrates, simulations were iterated for one million generations.

Finally, we performed simulations to assess whether sex-specific dominance evolves, starting from a population without dominance ($d_♀ = 0 = d_♂$). In this scenario, dominance is determined by two separate modifier loci $d_♀$ and $d_♂$, respectively. Alleles in these modifier loci are only expressed in their respective sex, act additively, and are unlinked to the locus coding for the trait z (full recombination). For the modifier loci, we use an expected mutational step size of 5 and a slightly higher mutation probability ($\mu_d = 5 \times 10^{-6}$) as we are only interested in the direction of dominance evolution. For the case of an X-linked locus, dominance is represented by $d_♀$, as only females can exhibit dominance at X-linked loci.

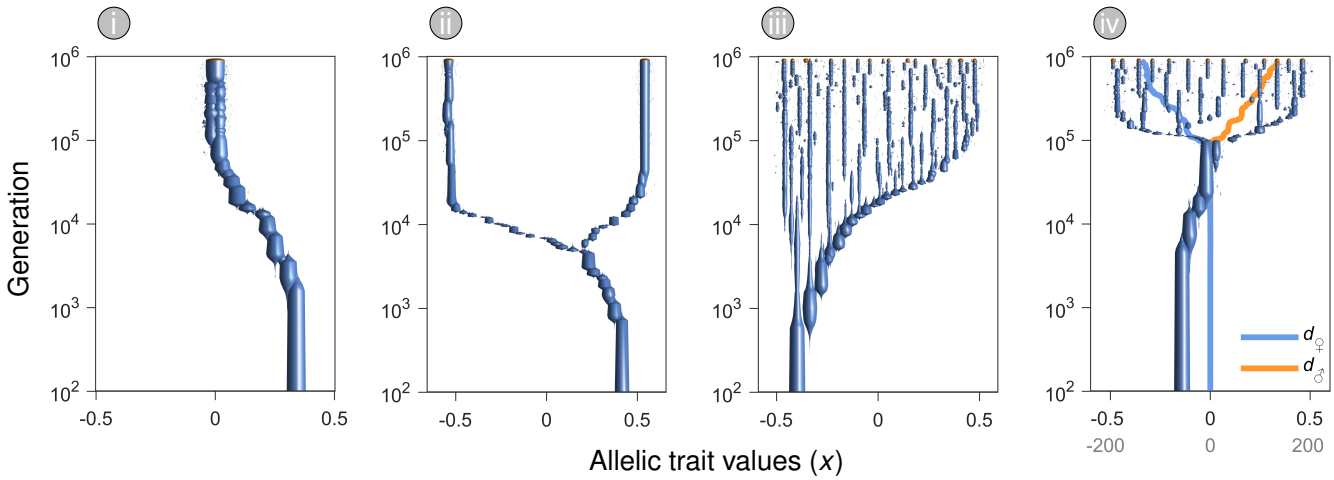

Figure 4. Examples of individual-based simulations of the evolution of allelic values at an autosomal locus under sexually antagonistic selection. (**i**), (**iii**) and (**iv**) show simulations under weak selection ($\sigma_♀^{-1} = 1 = \sigma_♂^{-1}$, analogous to Figure 1A), while (**ii**) is under strong selection ($\sigma_♀^{-1} = 2.5 = \sigma_♂^{-1}$, Figure 1C). (**i**) and (**ii**) are for the case of no dominance ($d_♀ = 0 = d_♂$), (**iii**) features strong sex-specific dominance ($d_♀ = -300$ and $d_♂ = 300$), while (**iv**) presents a simulation where dominance evolves, determined by two traits, $d_♀$ and $d_♂$, starting from additivity ($d_♀ = 0 = d_♂$). The average trait value of the female and male dominance is given by the solid coloured lines with values given in gray on the x-axis. Parameter values for each simulation are given by the location of the Roman numerals in Figure 5.

Empirical methods

To assess whether SA loci show an elevated occurrence of PAP, we used extant population genomic data from three different geographic populations of a model species in SA research: the seed beetle *Callosobruchus maculatus* (Sayadi et al., 2019). Briefly, populations were sequenced using a pool-seq approach, followed by a standard pipeline for read-mapping and SNP calling. We refer in full to Sayadi et al. (2019) for methodological details.

We developed a gene-specific index of PAP in the form of $\log P$ (see SI Appendix S3.1). The larger negative $\log P$ is for a given gene, the less consistent the data is with BAP and the more consistent it is with PAP.

Our inferential rationale follows two complimentary paths. First, we asked whether genes more likely to represent SA loci were also more likely to show PAP. Here, we both compared X-linked with autosomal loci and genes showing signs of persistent balancing selection with those not under such selection. The latter was achieved by selecting loci showing trans-population ("ancestral") polymorphism in the form of shared intermediate frequency polymorphism in all three populations, here defined as having at least one shared SNP with minor base frequency > 0.3 in all three population (Sayadi et al., 2019). Trans-population polymorphism is predicted for genes under persistent balancing selection (Fijarczyk and Babik, 2015) and studies of both fruit flies (Ruzicka et al., 2019) and seed beetles (Sayadi et al., 2019; Arnqvist and Sayadi, 2022) are consistent with an enrichment of SA loci in such genes.

Second, we inverted the inferential logic and asked whether genes showing a strong signal of PAP are enriched with genes encoding for known SA phenotypes. This is made possible in seed beetles by the fact that they represent an experimental model system for studies of sex-specific selection, and SA phenotypes are unusually well characterized (Arnqvist and Sayadi, 2022). Briefly, phenotypic selection on shared life-history traits is SA such that females show a lower optima for a pace-of-life syndrome (Arnqvist et al., 2022): lower metabolic rate, prolonged juvenile development, larger body size, lower adult activity and a longer life-span (Bilde et al., 2009; Berg and Mak-

lakov, 2012; Berger et al., 2014*a*,*b*, 2016; Arnqvist et al., 2017; Grieshop and Arnqvist, 2018). We first standardized $\log P$ within populations and then selected all outlier genes defined as showing a standardized $\log P < -5$ in any of the three populations. To identify over-representation of Gene Ontology terms among these genes, we used a hypergeometric test with a P-value cut-off 0.05 as implemented in the GOstats package v.2.46.0 (Falcon and Gentleman, 2007). Here, the gene universe was all polymorphic genes showing more than one well-supported SNP.

We fitted standard parametric linear models of $\log P$ to our population genomic data but also evaluated all inferential models using non-parametric resampling tests, based on 9999 random permutations. In all models, we used the total gene length and the number of SNPs for each gene as covariates. In models comparing X-linked and autosomal genes, we also included a population and gene specific measure of the pN/pS ratio as a covariate, to account for gene specific effects of relaxed selection due to differences in N_e between X-linked and autosomal genes (Sayadi et al., 2019). Genstat v.18.1.0.17005 was used for all statistical analyses.

Results

We first present our results for the case of an autosomal locus, and then continue to briefly describe the (very similar) results for the X-linked case.

Evolutionary attractor. We find that the evolutionary dynamics due to repeated invasion and fixation of novel mutant alleles initially leads toward a single allele x^* (given by Eq. S19), coding for the trait value z^*, which maximizes geometric mean survival across sexes, both for autosomal loci (in line with previous work, e.g. Charnov, 1982; Leimar, 2001) and for X-linked loci (SI Appendix S2.4). The trait value z^* is located between the female and male optima, at the exact midpoint under symmetric selection, or closer to the optimum of the sex that is under stronger selection (black dots in Fig. 1). The fact that in our model x^* is always an evolutionary attractor is somewhat sensitive to the functional form of the map from phenotypic trait z to survival w (here given by Eq. S2). For an equivalent model, Flintham et al. (2023) find, using a different functional form, that x^* can be an evolutionary repeller when the map from trait to sex-specific performance is accelerating. We suggest, however, that their functional form leading to this outcome is biologically unrealistic as it entails that the performance function is cusp-shaped at the sex-specific optimum.

Evolutionary branching. Once evolution reaches the intermediate allelic value, x^* one of two things can happen. If x^* is uninvadable by nearby mutant alleles, then it is an evolutionary endpoint at which a population monomorphic for this allele experiences stabilizing selection (Fig. 4i). Alternatively, if x^* is invadable by nearby mutant alleles, it is a point where allelic diversification ensues through evolutionary branching. A population monomorphic for this allele then experiences disruptive selection, which initially results in BAP (Fig. 4ii), but can, under conditions discussed below, generate PAPs through further branching events (Fig. 4iii).

In SI Appendix S2.5.1 we show that the condition for evolutionary branching can be written as

$$\frac{\delta^2}{4} + (d_{♂} - d_{♀})\frac{(\sigma_{♀}^2 + \sigma_{♂}^2)}{8} > \frac{(\sigma_{♀}^2 + \sigma_{♂}^2)^3}{8\sigma_{♀}^2\sigma_{♂}^2}, \quad [1]$$

where δ denotes the distance between the sex-specific optima. The first term on the left-hand side describes the variance among the sex-specific phenotypic optima. Thus, increasing differences between female and male optima facilitate evolutionary diversification. The second term describes the effect of sex-specific dominance. Sex-specific dominance facilitates evolutionary diversification if $d_{♂} - d_{♀} > 0$. This condition states that alleles have a larger effect on the trait value z in the sex where they are more beneficial. We refer to sex-specific dominance fulfilling this inequality as adaptive (e.g., as in Fig. 5C-E). Non-adaptive dominance ($d_{♂} - d_{♀} < 0$) hinders evolutionary diversification. The effect of sex-specific dominance increases with weaker selection ($\sigma_{♀}^2$ and $\sigma_{♂}^2$ large). The right-hand side of the inequal-

ity captures the effect of selection strength that is independent of sex-specific dominance. Under symmetry ($\sigma^2_{♀} = \sigma^2 = \sigma^2_{♂}$) this term simplifies to σ^2. In the general case, this term is increasing in $\sigma^2_{♀}$ and $\sigma^2_{♂}$ when the strength of selection in the two sexes is sufficiently symmetric ($\sigma^2_{♀} \approx \sigma^2_{♂}$) but decreases for strongly asymmetric selection. The combined effect of $\sigma^2_{♀}$ and $\sigma^2_{♂}$ through the second term on the left-hand side and the term on the right-hand side depends on $d_{♂} - d_{♀}$. Under symmetry ($\sigma^2_{♀} = \sigma^2 = \sigma^2_{♂}$), Condition 1 can be rewritten as

$$\frac{\delta^2}{4 - (d_{♂} - d_{♀})} > \sigma^2, \qquad [2]$$

showing that evolutionary diversification is favoured if σ^2 is sufficiently small (strong selection) or $d_{♂} - d_{♀}$ sufficiently large. If, furthermore, sex-specific dominance is absent, Condition 1 simplifies to $\delta^2/4 > \sigma^2$, which is the same condition as found in models of resource and habitat specialisation (e.g., Slatkin, 1979; Dieckmann and Doebeli, 1999; Kisdi and Geritz, 1999; Svardal et al., 2015; Schmid et al., 2024).

The condition for evolutionary branching in the absence of sex-specific dominance ($d_{♂} = d_{♀}$) has a useful geometric interpretation. For this, we note that the growth rate of a rare mutant allele y invading a resident population in which all individuals are homozygous for an allele x is given by the Shaw-Mohler equation (Eq. S10), which is a linear combination of the female and male survival of individuals heterozygote for y and x. A consequence of this linearity (Levins, 1968; Charnov, 1982; Rueffler et al., 2004) is that a population monomorphic for the intermediate allelic value x^* is uninvadable if the red curves shown in the lower panel of Figure 1 are concave (negative second derivative) at z^* (as shown in the first two panels). Vice versa, x^* is invadable, and therefore an evolutionary branching point, if this curve is convex at z^* (positive second derivative, third panel). A further consequence is that in a population with two segregating alleles $x_1 < x^* < x_2$ that code for

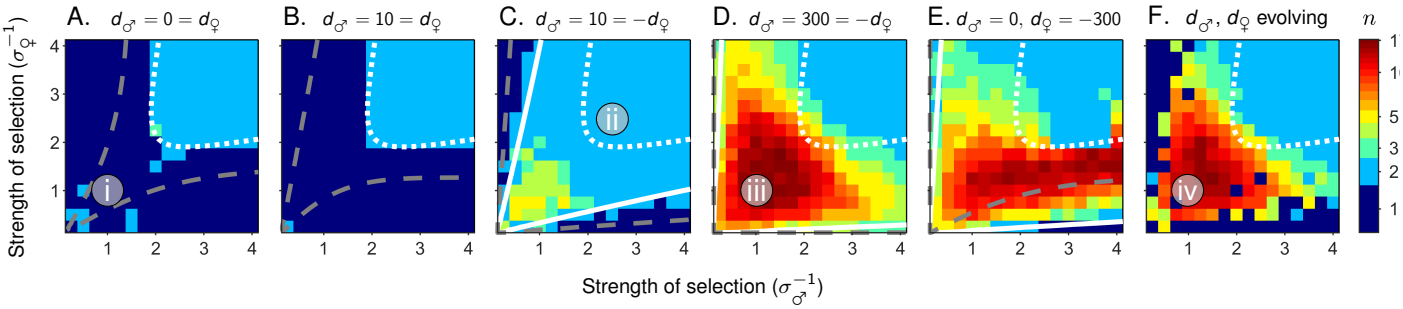

Figure 5. The number of coexisting alleles n at an autosomal locus under sexually antagonistic selection as a function of the strength of selection in the two sexes ($\sigma_{♀}^{-1}$ and $\sigma_{♂}^{-1}$) derived from individual-based simulations. The simulations explore different dominance regimes, as indicated above each panel. **A**. Additivity (corresponding to Fig. 2C and Fig. 3A); **B**. Partial dominance without sex-specificity (Fig. 2A). **C**. Weak adaptive dominance reversal (Fig. 2B and D, respectively). **D**. Full adaptive dominance reversal (Fig. 2A and E, respectively; see also Fig. 3C). **E**. Sex-limited dominance: beneficial dominance in females and additivity in males (Fig. 2A and C, respectively; see also Fig. 3B). **F**. Evolving dominance. Each pixel represents the outcome of a single simulation. Roman numerals are placed at parameter combinations for which a simulated evolutionary tree is shown in the corresponding panel in Figure 4. Hatched white lines delimit the threshold condition for polymorphism to emerge from evolutionary branching in the absence of sex-specific dominance (Equation S24 for $d_{♀} = d_{♂}$), with polymorphism evolving above and to the right of these lines. Solid white lines delimit the threshold condition for polymorphism to emerge from evolutionary branching given dominance as indicated above each panel (Equation S24). Dashed grey lines in **A**-**E** delimit the parameter region where the two specialist alleles can coexist, corresponding to results of Kidwell et al. (1977) (see main text for details). In **F**, polymorphism evolves across the entire parameter space (just as in **D**) given that dominance reversal evolves, which it does after a sufficiently long time.

the two sex specific optimal phenotypes or phenotypes in between these optima, the survival of homozygotes when averaged over the two sexes is higher than the average survival of heterozygotes (marginal underdominance). Thus, adaptive allelic diversification in the absence of sex-specific dominance is driven by female- and male-adapted alleles enjoying higher average survival than alleles that code for an intermediate phenotype. In contrast, if the allele x^* experiences stabilizing selection, then this is because the survival of individuals homozygous for this allele, when averaged over females and males, is higher than that of alleles more specialized for one sex.

The hatched white curves in Figure 5 show the combinations of female and male strength of selection at which the curves in the lower panel of Figure 1 change from concave to convex. Consequently, in the absence of sex-specific dominance ($d_{♂} = d_{♀}$, Figure 5A, B) allelic diversification is only possible above and to the right of the hatched white curves, and the alleles in the resulting BAP are maintained by balancing selection where the fitness of homozygote individuals, when averaged over the two sexes, is greater than that of heterozygotes.

Condition 1 indicates that the parameter region allowing for allelic diversification increases with increasing adaptive sex-specific dominance ($d_{♂} - d_{♀} > 0$). This is shown in Figure 5C-E, where polymorphism can emerge also below and to the left of the hatched white line. To understand this, we again make use of a geometrical argument. Under sex-specific dominance, heterozygote females and males carrying the same two alleles show different trait values z. Thus, the combination of female and male survival of such heterozygotes is no longer placed on the curves in the lower panel of Figure 1 but either above (if sex-specific dominance is adaptive) or below (if sex-specific dominance is maladaptive). As an example, the filled grey dots in the lower panel indicate female and male survival under full adaptive dominance reversal ($d_{♀}$ large negative and $d_{♂}$ large positive) for individuals heterozygote for the alleles coding for the female and male optimal phenotype, respectively. Thus, in a population with two segregating alleles $x_1 < x^* < x_2$ that code for the two sex-specific optimal phenotypes or phenotypes in between these optima, the survival of homozygotes, when averaged over the two sexes, is lower than the average survival of heterozygotes (marginal overdominance): heterozygous individuals enjoy an average survival that no single allele can achieve in homozygous individuals. Adaptive allelic diversification in the presence of sex-specific dominance for combinations of female and male survival strengths that lie below and to the left of the white hatched lines in Figure 1 is thus driven by heterozygote advantage: heterozygous individuals enjoy an average survival that no single allele can achieve in homozygous individuals. Moreover, with dominance reversal, heterozygote advantage also appears in the parameter region above and to the right of the hatched white lines in Figure 1C-F.

Even if only one sex experiences beneficial dominance and the other sex additive allelic effects, as illustrated in Figure 3B, allelic polymorphism can emerge in most of the parameter space (Fig. 5E). This occurs because a population monomorphic for x^* can then be invaded by any mutant allele more optimal for the sex not exhibiting additivity: the mutant allele initially always occurs in a heterozygote, experiencing equal survival to the resident homozygote in the sex with adaptive dominance and higher survival in the other. More generally, for sex-specific dominance to promote allelic diversity a reversal of dominance is not necessary; it is sufficient that one sex experiences more adaptive dominance than the other. This means that allelic polymorphism is promoted even if one sex exhibits detrimental dominance ($d_{♀} > 0$ or $d_{♂} < 0$), provided the other sex experiences stronger adaptive dominance to satisfy $d_{♂} - d_{♀} > 0$.

Allelic polymorphisms. Through individual-based simulations, we determine the final number of coexisting alleles, shown by the colour code in Figure 5, and their distribution in trait space. We first describe our result concerning the final number and conclude with some observations about the distribution.

We find that in the absence of sex-specific dominance, evolution results in at most two coexisting alleles (BAP), which occurs if the branching condition is met (above and to the right of the hatched white line in Fig. 5A,B; some simulation in A show three coexisting alleles, which is due to transient dynamics). This is because under marginal underdominance, one allele becomes specialized for each of the two sexes.

In contrast, in the presence of adaptive sex-specific dominance, we find that consecutive evolutionary branching events (as illustrated in Fig. 4iii) can result in more than two coexisting alleles (PAP, below and to the left of the hatched white lines but above and to the right of the solid white lines in Fig. 5C,D). Allelic diversity increases with increasing strength of sex-specific dominance (compare Fig. 5C with D). Furthermore, if sex-specific dominance is symmetric, allelic diversity is higher for symmetric and weak selection, while if sex-specific dominance is asymmetric, allelic diversity is higher when selection is stronger in the sex with weaker sex-specific dominance (compare Fig. 5D with E). High allelic diversity in these cases emerges because under marginal overdominance, each additional new rare allele initially enjoys the high marginal viability of heterozygotes. With each successive branching event, the proportion of homozygotes diminishes, thereby reducing the segregation load due to low fitness homozygotes. For instance, with ten equally frequent alleles, only 10% of individuals would be homozygous. Our finding corresponds to results from Kimura and Crow (1964), who show that under equal and high survival of heterozygotes in combination with equal and low survival of homozygotes, an arbitrary number of alleles can be maintained.

Adaptive sex-specific dominance does not result in more than two coexisting alleles if selection is strong and symmetric (as in Fig. 1C; above and to the right of the white hatched lines in Fig. 5C-F). In this case, the marginal survival of heterozygotes carrying two alleles on opposite sites of x^* drops sharply with increasing distance from the sex specific optima. Thus, the condition for coexistence outlined by Kimura and Crow (1964) is then violated because the heterozygote carrying the two maximally specialized alleles has a significantly higher marginal survival than any other heterozygote.

We now describe some observations about the distribution of allelic values in trait space. Figure S1 shows the maximum difference in allelic value between all coexisting alleles. Generally, the maximum difference is similar to the distance between the sex-specific phenotypic optima (as in Fig. 4ii-iv; yellow and green areas in Fig. S1). Results deviate from this rule if alleles act additively in at least one of the sexes (red areas in Fig. S1). For the case of additivity in both sexes, this result can be understood as follows. Here, only one allele reaches a sex-specific optima, generating a homozygote with optimal phenotype for one sex. For equal and strong selection in the two sexes, this allele occurs with frequency 3/4. However, the other, rarer allele evolves far beyond the optima for the other sex, such that the heterozygote, instead of the other homozygote, shows the optimal phenotype (as in Fig. 4v). This generates a higher frequency of 15/32 of high marginal survival genotypes, instead of 1/4, which would have been achieved by two alleles of equal frequency at the two optima. Analogous results have been found by Kisdi and Geritz (1999) in a model investigating allelic evolution in a population occupying two habitats.

The simulations in Figure 4iii,iv show that allelic values are eventually spread evenly across the trait space. This is representative for most parameter space in which PAPs evolve. Counterexamples are shown in Figure S3vi-viii. While we generally find only two coexisting alleles for parameter combinations above and to the right of the white hatched lines in Figure 5, panel (vi) corresponds to the small parameter region where allelic diversification results in PAPs. Panel (vii) and (viii) show that the distribution of allelic values can be highly skewed when adaptive dominance is present in one sex while alleles act additively in the other sex.

Evolving dominance. We here consider a scenario in which dominance in each sex ($d_{♀}$ and $d_{♂}$) is

determined by a separate modifier locus. These modifier loci coevolve with the locus determining the trait value z. Any mutation at the modifier loci that renders dominance more adaptive—corresponding to lower $d_{♀}$-values or higher $d_{♂}$-values—increases survival in the affected sex of individuals heterozygotic in the trait locus. Consequently, such mutations are always selected for in populations that are polymorphic in the trait locus. The modifier loci have no effect in individuals homozygotic in the trait locus, and are therefore effectively neutral in monomorphic populations.

In scenarios of strong symmetric selection, to the right and above the dashed white line in Figure 5F, we know from Figure 5A,B that a polymorphism in the trait locus evolves even in the absence of sex-specific dominance. Once a polymorphism is present, adaptive dominance reversal invariably evolves and the evolutionary outcome in this parameter region therefore closely resemble that in Figure 5D, where adaptive dominance reversal is assumed from the start.

In regions to the left and below the dashed white lines in Figure 5F, evolutionary branching is not expected without sex-specific dominance, and the trait locus evolves towards the intermediate allelic value x^*. At the same time, sex-specific dominance is favoured only in the presence of polymorphism at the trait locus. This interdependence creates a feedback loop where allelic monomorphism at the trait locus becomes stochastically unstable. On the one hand, mutation-drift dynamics introduces polymorphism around x^*, which then selects for alleles increasing adaptive sex-specific dominance. On the other hand, since alleles coding for dominance are selectively neutral in populations monomorphic for the trait locus, such alleles can drift to fixation, which then can select for polymorphism at the trait locus. These scenarios may require long periods of time before the coevolutionary process takes off. This is particularly true under asymmetric conditions where selection is weak in one sex and strong in the other, since then dominance has to drift to appreciable levels before polymorphism can evolve. This can be seen to the left and below the solid white lines in Figure 5C, where for polymorphism to evolve it is required that $d_{♂} - d_{♀} > 20$. These parameter regions correspond to simulations in Figure 5F where simulation runs ended before polymorphism in the trait locus evolved (seen as dark blue pixels).

Dominance can also evolve via another route. Before evolution becomes monomorphic for x^*, BAPs consisting of two alleles x_1 and x_2 on opposite sites of x^* can occur. These alleles are maintained by balancing selection until a new mutant allele closer to x^* invades and replaces one or both existing alleles, leading to the eventual

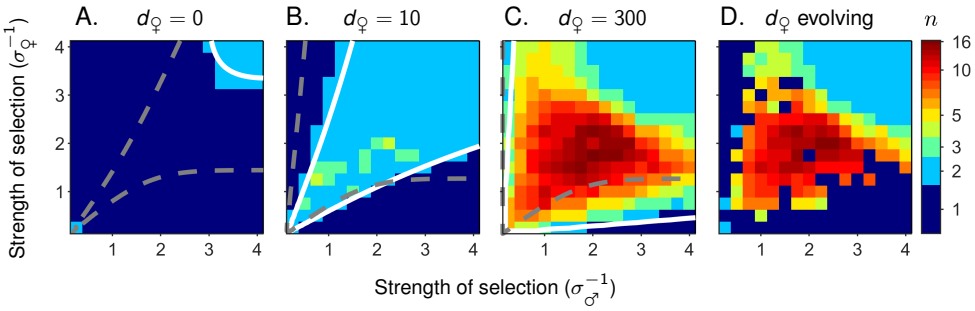

Figure 6. The number of coexisting alleles n at an X-linked locus under sexually antagonistic selection as a function of the strength of selection in the two sexes ($\sigma_{♀}^{-1}$ and $\sigma_{♂}^{-1}$) derived from individual-based simulations. The simulations explore different dominance regimes, as indicated above each panel. **A.** Additivity (corresponding to Fig. 2C and Fig. 3A). **B.** Partial dominance in females (Fig. 2B). **C.** Full dominance in females (Fig. 2A). **D.** Evolving dominance. Each pixel represents the outcome of a single simulation. Solid white lines delimit the threshold condition for polymorphism to emerge from evolutionary branching (Eq. S26), with polymorphism evolving above and to the right these lines. Dashed grey lines delimit the parameter region where the two specialist alleles can coexist, corresponding to results of Kidwell et al. (1977) for the X-linked case.

loss of BAP and stabilization of the population at x^*. The emergence and subsequent loss of such transient BAP can be observed in Figure 4i within the time interval between 10^5 and 10^6. This phase of transient BAP is a window of opportunity for the evolution of adaptive dominance reversal. If this indeed occurs, then selection on the two coexisting alleles can change from stabilizing to disruptive, starting the coevolution of sex-specific dominance and trait polymorphism, as illustrated in Figure 4iv.

Coexistence of specialist alleles. We also investigate the conditions under which two specialist alleles can coexist, disregarding input of intermediate alleles by mutation. This static approach allows us to align our model with the classic results presented by Kidwell et al. (1977). In our model, the allele optimal in each sex yields homozygotes with a survival probability of 1 in that sex and a reduced survival of $1 - s_{♀}$ in the other sex (as given by the intersection of the hatched vertical lines and the coloured lines in the upper panel of Fig. 1). We note that our model differs from the above-mentioned study in that we model dominance as acting at the level of the phenotypic trait z, rather than directly at the level of viability w. Despite this difference, the dashed gray lines in Figure 5A and C correspond closely to the findings presented in Figure 1 and 3F of Kidwell et al. (1977).

Importantly, the capacity for specialist alleles to coexist is neither necessary nor sufficient for the emergence of allelic polymorphism at an evolutionary branching point: the parameter region where allelic polymorphism arises is a subset of the parameter region where specialist alleles can coexist in Figure 5A-D, while the opposite holds true in Figure 5E.

X-linked loci. Figure 6 is analogous to Figure 5 and summarises the results for the case of sexually antagonistic selection acting at an X-linked locus. The condition for evolutionary branching is given by Equation S26 in the Supplementary Information and corresponds to the solid white lines in Figure 5A-C. These results show that the condition for the emergence of allelic polymorphism is significantly more stringent in X-linked loci compared to autosomal loci, particularly in the absence of adaptive dominance. The reason is that in the case of X-linked loci, male adapted alleles occur with probability 2/3 in females and males can inherent such loci only from their mother where they cause reduced survival if homozygous or in the absence of adaptive sex-specific dominance. Note, however, that since dominance is only expressed by females, allelic polymorphism is favoured whenever $d_{♀} < 0$, corresponding to female beneficial alleles being dominant in females. Given that polymorphism evolves, the final number of alleles is similar to the autosomal case.

Empirical results

The gene-specific pattern of variation across polymorphic loci was less consistent with BAP for X-linked genes relative to autosomal genes (California: $F_{1,8493} = 110.42$, $P < 0.001$, $P_{\text{perm}} < 0.001$; Brazil: $F_{1,8040} = 36.99$, $P < 0.001$, $P_{\text{perm}} < 0.001$; Yemen: $F_{1,8559} = 149.47$, $P < 0.001$, $P_{\text{perm}} < 0.001$). The pattern of variation across polymorphic loci was also significantly less consistent with BAP for genes showing shared intermediate frequency polymorphism relative to those that did not, in two out of the three populations (Fig. 7, California: $F_{1,8494} = 10.8$, $P < 0.001$, $P_{\text{perm}} = 0.024$; Brazil: $F_{1,8041} = 0.20$, $P = 0.654$, $P_{\text{perm}} = 0.729$; Yemen: $F_{1,8560} = 17.22$, $P < 0.001$, $P_{\text{perm}} = 0.007$). This suggests that older polymorphisms exhibit increased signals of PAPs, and is consistent with our prediction that balancing selection in SA loci, over time, should lead to the evolution of PAP in such genes for a large part of the parameter space. We note that the tenet that genes showing shared intermediate frequency polymorphism are enriched with SA loci is supported by functional enrichment analyses, sex-specific expression (Sayadi et al., 2019) and the pattern of differentiation (Arnqvist and Sayadi, 2022).

Our set of outlier genes, showing the strongest evidence for PAP, included 64 genes in total, of which nine showed shared polymorphism across all three populations. For the nine shared genes,

we performed a BLASTn search against the NCBI non-redundant nucleotide database, with default parameters and without filtering for low complexity regions. Potential hits were then manually curated. Seven genes yielded no significant hits. One matched a gene annotated as a zinc finger protein gene and one a circadian period protein gene. The latter is noteworthy given that circadian period genes are essential for biological clock functions, involving locomotor activity and the timing of eclosion, which are both known to be under SA selection in *C. maculatus* (Arnqvist and Tuda, 2010; Berger et al., 2014*a*). The functional enrichment analysis of the full set of 64 genes identified a series of significantly overrepresented Gene Ontology (GO) terms (see SI Appendix S3.2). These included an over-representation of genes involved in various aspects of metabolic processes. Strikingly, four out of five significant GO terms for cellular components are directly involved in ATP production. Similarly, a majority of the significant GO terms for biological processes are directly involved in energy metabolism, such as ATP production, carbohydrate metabolism, carbohydrate biosynthesis and other key metabolic processes.

Discussion

We model for the first time the joint evolution of allelic diversity and sex-specific dominance for a shared phenotypic trait where males and females have different optima. Our analyses of this SA pleiotropy in part confirm previous modelling efforts, such that additivity and equal dominance between the sexes can generate a stable bi-allelic dimorphism only when selection is relatively strong and symmetric between the sexes (e.g., Kidwell et al., 1977; Connallon and Clark, 2012; Arnqvist et al., 2014; Flintham et al., 2023), but they also generate a series of novel insights. We show that sex-specific dominance for the shared trait evolves readily when allowed (as in Spencer and Priest, 2016), and this has several important implications.

First, sex-specific dominance for trait expression significantly widens the parameter space under which polymorphism evolves and is maintained. Further, full adaptive dominance reversal, where alleles are fully dominant in one sex and fully recessive in the other in a manner aligned with selection, is not required for this effect, but it is more generally true whenever adaptive dominance is sex-specific such as when allelic effects show additivity in one sex and some degree of dominance in the other (see also Brud, 2023). In an analysis of the effects of marginal overdominance resulting

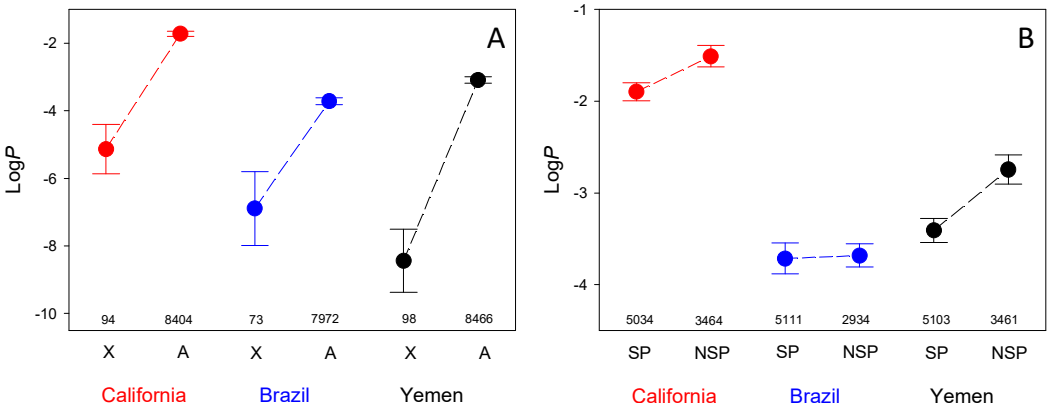

Figure 7. The strength of the signal for PAP in gene sets in three different populations of seed beetles. The figure shows predicted mean (±SE) $\log P$ value, where larger negative values are more consistent with PAP. **A**. The pattern of genetic variation in X-linked genes (X) is overall more consistent with PAP than that of autosomal (A) genes. **B**. Genes showing shared intermediate frequency polymorphism in three populations (SP), a characteristic of persistent balancing selection, exhibit a pattern of genetic variation more consistent with PAPs compared to those genes that do not (NSP) in two out of three populations. Numbers represents the number of genes in each set.

from temporally fluctuating selection, Wittmann et al. (2017) similarly found that relatively minor differences in context-specific adaptive dominance for traits under fluctuating selection is sufficient to promote the maintenance of polygenic polymorphism. The fact that we observe sex-specific dominance emerging in our model is, although consequential, perhaps not surprising: the evolution of adaptive dominance is predicted when polymorphism is maintained by marginal overdominance, as this increases heterozygote fitness (Fisher, 1931). The degree to which the evolution of dominance is constrained has been a matter of some debate (Otto and Bourguet, 1999; Grieshop et al., 2024), but it is clear that sex-specific dominance for phenotypic traits could emerge either through nonlinearities in the manner in which allelic effects are translated into phenotypes (Wright, 1934; Kacser and Burns, 1981; Otto and Bourguet, 1999; Reid, 2022) or through dominance modifiers (Spencer and Priest, 2016; Grieshop et al., 2024).

Second, unlike previous theory studying the implications of sex-specific dominance, our model is not restricted to BAP. This relaxation offers substantial novel insights. In much of the parameter space, we show that a locus under SA selection can recruit more than two segregating alleles such that polymorphism becomes polyallelic. The general mechanism promoting PAP is quite intuitive. Under marginal overdominance due to sex-specific dominance, a novel allele can invade in a BAP background simply because it is initially rare and will thus find itself expressed in a heterozygous state most of the time. In theory, it is well known that marginal overdominance generally tends to promote the evolution and maintenance of PAP (e.g., Kimura and Crow, 1964; Siljestam and Rueffler, 2023) and this should be true also for loci under SA selection (Gavrilets and Waxman, 2002; Haygood, 2004). Our analyses show that, given enough time and large population size, a large number of SA alleles can indeed emerge and coexist in a population. We note that PAP will greatly reduce segregation load, often referred to as gender load in this context (Rice and Chippindale, 2002), as the fraction of the population that is homozygote is low under PAP.

Although a few cases of PAP have been documented in candidate SA genes (Barson et al., 2015; Schmidt et al., 2010; Hawkes et al., 2016; Wagstaff and Begun, 2005; Lonn et al., 2017), relevant empirical data is somewhat limited due to the technical limitations of short read sequencing data and, not the least, the practical problems involved in the detection of segregating low-frequency variants. We introduce a simple method to estimate the empirical support for PAP in samples of sequencing reads from pools of individuals (SI Appendix S3.1), which we suggest provides a cost-efficient way to assess genome-wide PAP. We employ this method in a seed beetle species which is an established model system for SA selection, and show that the signal for PAP is elevated in X-linked compared with autosomal genes and in genes showing shared polymorphism across populations. Most importantly, genes showing the strongest hallmarks of PAP are significantly enriched with genes related to metabolic "pace-of-life" phenotypes shared between the sexes and known to be SA in this system (e.g., Berger et al., 2016; Arnqvist et al., 2022). We suggest that these findings provide at least provisional support for the predictions of our model.

In this context, regions that affect gene expression are particularly interesting. Pronounced sexual dimorphism in gene expression is near ubiquitous in gonochorists and both theory (Connallon and Knowles, 2005; Rowe et al., 2018; Tosto et al., 2023) and empirical data (Innocenti and Morrow, 2010; Hollis et al., 2014; Wong and Holman, 2023) suggest that regions affecting gene expression are often under, or have at least experienced a history of, SA selection. Moreover, several recent studies have documented widespread sex-specific dominance in gene expression (Puixeu et al., 2023; Mishra et al., 2022; Kaufmann et al., 2024), suggesting that regulatory regions may be enriched with loci showing segregating SA genetic variation. Several genomic regions with putative regulatory functions, such as mini- and microsatellites, show pronounced PAP and sometimes appear to be under balancing SA selection (e.g., Lonn et al., 2017). When superimposed on the results of our model,

these observations suggest that a sizeable fraction of standing SA genetic variance for fitness (Connallon and Matthews, 2019) may actually be caused by PAP in regulatory loci (Wright et al., 2018; Kaufmann et al., 2024).

A third insight from our model is that the evolution of sex-specific dominance promotes the maintenance of polymorphism even when selection is relatively weak. Although this confirms similar findings in previous models (e.g., Kidwell et al., 1977; Connallon and Clark, 2012; Arnqvist et al., 2014) the fact that weak selection conditions were particularly prone to generate PAP is a novel finding that may seem counterintuitive. It results from weak selection being more permissive to a greater allelic diversity maintained by heterozygote advantage: under strong selection, the highest fitness heterozygote essentially outcompetes others, leaving the population in a state of BAP.

In contrast to previous theoretical evaluations of sexually antagonistic pleiotropy, sex-specific dominance does not emerge from curved fitness functions (Connallon and Clark, 2014; Flintham et al., 2023) in our modelling approach. Instead, we assume that dominance occurs for trait expression (see also Wittmann et al., 2017) and we also allow sex-specific dominance to evolve. Although dominance reversal for fitness is indeed predicted under curved fitness landscapes (Fry, 2010; Manna et al., 2011; Connallon and Chenoweth, 2019), most documented cases of sex-specific dominance involve dominance effects on phenotypes. This is true for age at maturation in salmon (Barson et al., 2015), morphology in water striders (Fairbairn et al., 2023), immune function in fruit flies (Geeta Arun et al., 2021), migratory behaviour in rainbow trout (Pearse et al., 2019) and transcript abundance in fruit flies (Puixeu et al., 2023; Mishra et al., 2022) and beetles (Kaufmann et al., 2024). This suggests that documented cases of sex-specific dominance for fitness components (Grieshop and Arnqvist, 2018; Mérot et al., 2020) may to a large extent emerge from underlying differences in dominance for trait expression, which we believe substantiates our approach.

Classic theory suggests that the X-chromosome should be enriched with SA loci (Rice, 1984), although subsequent models have shown that this is not necessarily true under sex-specific dominance reversal (e.g., Fry, 2010). Moreover, empirical data is somewhat ambiguous (Dean and Mank, 2014; Ruzicka and Connallon, 2020). Our analyses show that the conditions favouring polymorphism under additive genetic effects are more restrictive in X-linked loci compared to autosomal loci (see Fig. 6A and Fig. 5A, respectively). However, in the presence of dominance, conditions for polymorphism can be less restrictive in X-linked loci (compare Fig. 6B with Fig. 5B). Generally, dominance without sex-specificity may be common and much less constrained than the evolution of sex-specific dominance. Since dominance in X-linked loci is equally effective in promoting PAPs as adaptive sex-specific dominance in autosomal loci (compare Fig. 6C and Fig. 5D), PAPs in X-linked SA loci might indeed evolve more readily compared to autosomal loci, aligning with our empirical observations shown in Figure 7A.

Generally, the evolution of context-specific dominance requires some time. Since balancing selection increases the lifespan of alleles and promotes intermediate frequency polymorphism, it sets the stage for more persistent selection for adaptive dominance in heterozygotes (Fisher, 1931; Otto and Bourguet, 1999). Once adaptive context-specific dominance evolves, this introduces or strengthen marginal overdominance and thus further promote the maintenance of allelic diversity. For SA loci, this predicts a dynamic scenario in which novel mutations appear and can be maintained for some time through marginal overdominance in a population. Whether transient polymorphisms are then lost or survive as evolutionary stable polymorphisms will depend on whether and how sex-specific dominance subsequently evolves. Our simulations clearly illustrate this coevolutionary process (e.g. Figure4iv). We suggest that time will thus sift novel SA mutations such that standing SA genetic variation for fitness, which is often sizeable (Connallon and Matthews, 2019), should at any point in time be enriched with loci showing PAP and adaptive sex-specific dominance.

Appendix

The trait value z of an individual with alleles x_i and x_j is given by

$$z_k(x_i, x_j) = \frac{\delta}{d_k} \ln\left(\frac{e^{d_k x_i} + e^{d_k x_j}}{2}\right). \qquad \text{[A1]}$$

Here, δ denotes the distance between the sex-specific phenotypic optima and the dominance parameter d_k governs the degree and direction of dominance for sex $k \in \{♀, ♂\}$. As this equation is not defined for $d = 0$, we replace the right-hand side with its limit for $d \to 0$, namely $\delta(x_i + x_j)/2$. Hence, for $d = 0$ the two alleles act additively. Equation A1 defines a dominance hierarchy for any two alleles, as shown in Figure 2.

Acknowledgements

We thank Ahmed Sayadi for help with the bioinformatic work.

Funding: This research was supported by the Swedish Research Council (2019-03611; 2023-03730), the Program for Animal Ecology at the Department of Ecology and Genetics, Uppsala University, and Stiftelsen för Zoologisk Forskning.

References

Arnqvist, G. 2011. Assortative mating by fitness and sexually antagonistic genetic variation. Evolution, 65:2111–2116.

Arnqvist, G., J. Rönn, C. Watson, J. Goenaga, and E. Immonen. 2022. Concerted evolution of metabolic rate, economics of mating, ecology, and pace of life across seed beetles. Proceedings of the National Academy of Sciences, 119:e2205564119.

Arnqvist, G., and L. Rowe. 2005. Sexual conflict. Princeton University Press.

Arnqvist, G., and A. Sayadi. 2022. A possible genomic footprint of polygenic adaptation on population divergence in seed beetles? Ecology and Evolution, 12:e9440.

Arnqvist, G., B. Stojković, J. L. Rönn, and E. Immonen. 2017. The pace-of-life: A sex-specific link between metabolic rate and life history in bean beetles. Functional Ecology, 31:2299–2309.

Arnqvist, G., and M. Tuda. 2010. Sexual conflict and the gender load: correlated evolution between population fitness and sexual dimorphism in seed beetles. Proceedings of the Royal Society B: Biological Sciences, 277:1345–1352.

Arnqvist, G., N. Vellnow, and L. Rowe. 2014. The effect of epistasis on sexually antagonistic genetic variation. Proceedings of the Royal Society B: Biological Sciences, 281:20140489.

Barson, N. J., T. Aykanat, K. Hindar, M. Baranski, G. H. Bolstad, P. Fiske, C. Jacq, A. J. Jensen, S. E. Johnston, S. Karlsson, et al. 2015. Sex-dependent dominance at a single locus maintains variation in age at maturity in salmon. Nature, 528:405.

Berg, E. C., and A. A. Maklakov. 2012. Sexes suffer from suboptimal lifespan because of genetic conflict in a seed beetle. Proceedings of the Royal Society B: Biological Sciences, 279:4296–4302.

Berger, D., E. C. Berg, W. Widegren, G. Arnqvist, and A. A. Maklakov. 2014*a*. Multivariate intralocus sexual conflict in seed beetles. Evolution, 68:3457–3469.

Berger, D., K. Grieshop, M. I. Lind, J. Goenaga, A. A. Maklakov, and G. Arnqvist. 2014*b*. Intralocus sexual conflict and environmental stress. Evolution, 68:2184–2196.

Berger, D., I. Martinossi-Allibert, K. Grieshop, M. I. Lind, A. A. Maklakov, and G. Arnqvist. 2016. Intralocus sexual conflict and the tragedy of the commons in seed beetles. The American Naturalist, 188:E98–E112.

Bilde, T., A. Foged, N. Schilling, and G. Arnqvist. 2009. Postmating sexual selection favors males that sire offspring with low fitness. science, 324:1705–1706.

Billiard, S., and V. Castric. 2011. Evidence for fisher's dominance theory: how many 'special cases'? Trends in Genetics, 27:441–445.

Billiard, S., V. Castric, and V. Llaurens. 2021. The integrative biology of genetic dominance. Biological Reviews, 96:2925–2942.

Brud, E. 2023. Dominance and the potential for seasonally balanced polymorphism. bioRxiv, 2023.11.20.567918.

Champagnat, N., R. Ferrière, and S. Méléard. 2006. Unifying evolutionary dynamics: from individual stochastic processes to macroscopic models. Theoretical Population Biology, 69:297–321.

Charlesworth, B. 2015. Causes of natural variation in fitness: evidence from studies of *Drosophila* populations. Proceedings of the National Academy of Sciences, 112:1662–1669.

Charlesworth, B., and K. A. Hughes. 2000. The maintenance of genetic variation in life-history traits. Pages 369–392 *in* Evolutionary genetics: from molecules to morphology. Cambridge University Press.

Charnov, E. L. 1982. The Theory of Sex Allocation. Princeton university press, Princeton.

Chen, J., V. Nolte, and C. Schlötterer. 2015. Temperature stress mediates decanalization and dominance of gene expression in *Drosophila melanogaster*. PLoS genetics, 11:e1004883.

Connallon, T., and S. F. Chenoweth. 2019. Dominance reversals and the maintenance of genetic variation for fitness. PLoS Biology, 17:e3000118.

Connallon, T., and A. G. Clark. 2012. A general population genetic framework for antagonistic selection that accounts for demography and recurrent mutation. Genetics, 190:1477–1489.

Connallon, T., and A. G. Clark. 2014. Balancing selection in species with separate sexes: insights from fisher's geometric model. Genetics, 197:991–1006.

Connallon, T., and L. L. Knowles. 2005. Intergenomic conflict revealed by patterns of sex-biased gene expression. Trends in Genetics, 21:495–499.

Connallon, T., and G. Matthews. 2019. Cross-sex genetic correlations for fitness and fitness components: connecting theoretical predictions to empirical patterns. Evolution Letters, 3:254–262.

Curtsinger, J. W., P. M. Service, and T. Prout. 1994. Antagonistic pleiotropy, reversal of dominance, and genetic polymorphism. The American Naturalist, 144:210–228.

Dean, R., and J. E. Mank. 2014. The role of sex chromosomes in sexual dimorphism: discordance between molecular and phenotypic data. Journal of Evolutionary Biology, 27:1443–1453.

Dercole, F., and S. Rinaldi. 2008. Analysis of evolutionary processes: the adaptive dynamics approach and its applications: the adaptive dynamics approach and its applications. Princeton University Press.

Dieckmann, U., and M. Doebeli. 1999. On the origin of species by sympatric speciation. Nature, 400:354–357.

Doebeli, M. 2011. Adaptive Diversification (MPB-48). Princeton University Press.

Fairbairn, D. J., D. A. Roff, and M. E. Wolak. 2023. Tests for associations between sexual dimorphism and patterns of quantitative genetic variation in the water strider, aquarius remigis. Heredity, 131:109–118.

Falcon, S., and R. Gentleman. 2007. Using gostats to test gene lists for go term association. Bioinformatics, 23:257–258.

Fijarczyk, A., and W. Babik. 2015. Detecting balancing selection in genomes: limits and prospects. Molecular ecology, 24:3529–3545.

Fisher, R. A. 1930. The genetical theory of natural selection. Oxford University Press.

Fisher, R. A. 1931. The evolution of dominance. Biological Reviews of the Cambridge Philosophical Society, 6:345–368.

Flintham, E., V. Savolainen, S. Otto, M. Reuter, and C. Mullon. 2023. The maintenance of genetic polymorphism in sexually antagonistic traits. bioRxiv, 2023.10.10.561678.

Fry, J. D. 2010. The genomic location of sexually antagonistic variation: some cautionary projects. Evolution, 64:1510–1516.

Gavrilets, S., and D. Waxman. 2002. Sympatric speciation by sexual conflict. Proceedings of the National Academy of Sciences, 99:10533–10538.

Geeta Arun, M., A. Agarwala, Z. A. Syed, M. Kashyap, S. Venkatesan, T. S. Chechi,

V. Gupta, and N. G. Prasad. 2021. Experimental evolution reveals sex-specific dominance for surviving bacterial infection in laboratory populations of *Drosophila melanogaster*. Evolution Letters, 5:657–671.

Geritz, S. A. H., É. Kisdi, G. Meszéna, and J. A. J. Metz. 1998. Evolutionarily singular strategies and the adaptive growth and branching of the evolutionary tree. Evolutionary Ecology, 12:35–57.

Gibson, J. R., A. K. Chippindale, and W. R. Rice. 2002. The x chromosome is a hot spot for sexually antagonistic fitness variation. Proceedings of the Royal Society of London. Series B: Biological Sciences, 269:499–505.

Glaser-Schmitt, A., M. J. Wittmann, T. J. Ramnarine, and J. Parsch. 2021. Sexual antagonism, temporally fluctuating selection, and variable dominance affect a regulatory polymorphism in *Drosophila melanogaster*. Molecular Biology and Evolution, 38:4891–4907.

Grieshop, K., and G. Arnqvist. 2018. Sex-specific dominance reversal of genetic variation for fitness. PLoS biology, 16:e2006810.

Grieshop, K., E. K. Ho, and K. R. Kasimatis. 2024. Dominance reversals: The resolution of genetic conflict and maintenance of genetic variation. Proceedings of the Royal Society B: Biological Sciences, 291:20232816.

Hawkes, M., C. Gamble, E. Turner, M. Carey, N. Wedell, and D. Hosken. 2016. Intralocus sexual conflict and insecticide resistance. Proceedings of the Royal Society B: Biological Sciences, 283:20161429.

Haygood, R. 2004. Sexual conflict and protein polymorphism. Evolution, 58:1414–1423.

Hollis, B., D. Houle, Z. Yan, T. J. Kawecki, and L. Keller. 2014. Evolution under monogamy feminizes gene expression in *Drosophila melanogaster*. Nature communications, 5:3482.

Huber, C. D., A. Durvasula, A. M. Hancock, and K. E. Lohmueller. 2018. Gene expression drives the evolution of dominance. Nature communications, 9:2750.

Innocenti, P., and E. H. Morrow. 2010. The sexually antagonistic genes of *Drosophila melanogaster*. PLoS biology, 8:e1000335.

Kacser, H., and J. A. Burns. 1981. The molecular basis of dominance. Genetics, 97:639–666.

Kaufmann, P., J. Rönn, E. Immonen, and G. Arnqvist. 2024. Sex-specific dominance of gene expression in seed beetles. Manuscript in review.

Kidwell, J., M. Clegg, F. Stewart, and T. Prout. 1977. Regions of stable equilibria for models of differential selection in the two sexes under random mating. Genetics, 85:171–183.

Kimura, M., and J. F. Crow. 1964. The number of alleles that can be maintained in a finite population. Genetics, 49:725–738.

Kisdi, É., and S. A. H. Geritz. 1999. Adaptive dynamics in allele space: evolution of genetic polymorphism by small mutations in a heterogeneous environment. Evolution, pages 993–1008.

Leimar, O. 2001. Evolutionary change and darwinian demons. Selection, 2:65–72.

Levins, R. 1968. Evolution in changing environments: some theoretical explorations. 2. Princeton University Press, Princeton, New Jersey.

Lewontin, R., L. Ginzburg, and S. Tuljapurkar. 1978. Heterosis as an explanation for large amounts of genic polymorphism. Genetics, 88:149–169.

Lonn, E., E. Koskela, T. Mappes, M. Mokkonen, A. M. Sims, and P. C. Watts. 2017. Balancing selection maintains polymorphisms at neurogenetic loci in field experiments. Proceedings of the National Academy of Sciences, 114:3690–3695.

Manna, F., G. Martin, and T. Lenormand. 2011. Fitness landscapes: an alternative theory for the dominance of mutation. Genetics, 189:923–937.

Meiklejohn, C. D., J. D. Coolon, D. L. Hartl, and P. J. Wittkopp. 2014. The roles of cis-and trans-regulation in the evolution of regulatory incompatibilities and sexually dimorphic gene expression. Genome Research, 24:84–95.

Mérot, C., V. Llaurens, E. Normandeau, L. Bernatchez, and M. Wellenreuther. 2020. Balancing selection via life-history trade-offs maintains an inversion polymorphism in a seaweed fly. Nature communications, 11:670.

Metz, J. A. J. 2008. Fitness. Pages 1599–1612 *in* S. E. Jorgensen and B. Fath, eds. Encyclopedia of ecology. Oxford: Elsevier, available online as IIASA Interim Report IR-06-061.

Metz, J. A. J., R. M. Nisbet, and S. A. H. Geritz. 1992. How should we define 'fitness' for general ecological scenarios? Trends in Ecology & Evolution, 7:198–202.

Mishra, P., T. S. Barrera, K. Grieshop, and A. F. Agrawal. 2022. Cis-regulatory variation in relation to sex and sexual dimorphism in drosophila melanogaster. bioRxiv, 2022.09.20.508724.

Mitchell-Olds, T., J. H. Willis, and D. B. Goldstein. 2007. Which evolutionary processes influence natural genetic variation for phenotypic traits? Nature Reviews Genetics, 8:845–856.

Otto, S. P., and D. Bourguet. 1999. Balanced polymorphisms and the evolution of dominance. The American Naturalist, 153:561–574.

Patten, M. M., and D. Haig. 2009. Maintenance or loss of genetic variation under sexual and parental antagonism at a sex-linked locus. Evolution, 63:2888–2895.

Pearse, D. E., N. J. Barson, T. Nome, G. Gao, M. A. Campbell, A. Abadía-Cardoso, E. C. Anderson, D. E. Rundio, T. H. Williams, K. A. Naish, et al. 2019. Sex-dependent dominance maintains migration supergene in rainbow trout. Nature ecology & evolution, 3:1731–1742.

Priklopil, T., and L. Lehmann. 2020. Invasion implies substitution in ecological communities with class-structured populations. Theoretical population biology, 134:36–52.

Prout, T. 2000. How well does opposing selection maintain variation. Pages 157—181 *in* Evolutionary genetics: from molecules to morphology. Cambridge University Press.

Puixeu, G., A. Macon, and B. Vicoso. 2023. Sex-specific estimation of cis and trans regulation of gene expression in heads and gonads of *Drosophila melanogaster*. G3: Genes, Genomes, Genetics, 13:jkad121.

Reid, J. M. 2022. Intrinsic emergence and modulation of sex-specific dominance reversals in threshold traits. Evolution, 76:1924–1941.

Reinhold, K. 1998. Sex linkage among genes controlling sexually selected traits. Behavioral Ecology and Sociobiology, 44:1–7.

Rice, W. R. 1984. Sex chromosomes and the evolution of sexual dimorphism. Evolution, 38:735–742.

Rice, W. R., and A. K. Chippindale. 2002. The evolution of hybrid infertility: perpetual coevolution between gender-specific and sexually antagonistic genes. Genetics of mate choice: from sexual selection to sexual isolation, pages 179–188.

Rowe, L., S. F. Chenoweth, and A. F. Agrawal. 2018. The genomics of sexual conflict. The American Naturalist, 192:274–286.

Rueffler, C., T. J. M. Van Dooren, and J. A. J. Metz. 2004. Adaptive walks on changing landscapes: Levins' approached extended. Theoretical Population Biology, 65:165–178.

Ruzicka, F., and T. Connallon. 2020. Is the x chromosome a hot spot for sexually antagonistic polymorphisms? biases in current empirical tests of classical theory. Proceedings of the Royal Society B, 287:20201869.

Ruzicka, F., M. S. Hill, T. M. Pennell, I. Flis, F. C. Ingleby, R. Mott, K. Fowler, E. H. Morrow, and M. Reuter. 2019. Genome-wide sexually antagonistic variants reveal long-standing constraints on sexual dimorphism in fruit flies. PLoS Biology, 17:e3000244.

Sayadi, A., A. Martinez Barrio, E. Immonen, J. Dainat, D. Berger, C. Tellgren-Roth, B. Nystedt, and G. Arnqvist. 2019. The genomic footprint of sexual conflict. Nature ecology & evolution, 3:1725–1730.

Schlötterer, C., R. Tobler, R. Kofler, and V. Nolte. 2014. Sequencing pools of individuals—mining genome-wide polymorphism data without big funding. Nature Reviews Genetics, 15:749–763.

Schmid, M., C. Rueffler, L. Lehmann, and C. Mullon. 2024. Resource variation within and between patches: Where exploitation competition, local adaptation, and kin selection meet. The American Naturalist, 203:E19–E34.

Schmidt, J. M., R. T. Good, B. Appleton, J. Sherrard, G. C. Raymant, M. R. Bogwitz, J. Martin, P. J. Daborn, M. E. Goddard, P. Batterham, et al. 2010. Copy number variation and transposable elements feature in recent, ongoing adaptation at the cyp6g1 locus. PLoS genetics, 6:e1000998.

Shaw, R. F., and J. D. Mohler. 1953. The selective significance of the sex ratio. The American Naturalist, 87:337–342.

Siljestam, M., and C. Rueffler. 2023. Heterozygote advantage can explain the extraordinary diversity of immune genes. bioRxiv, 347344.

Slatkin, M. 1979. Frequency- and density-dependent selection on a quantitative trait. Genetics, 93:755–771.

Spencer, H. G., and C. Mitchell. 2016. The selective maintenance of allelic variation under generalized dominance. G3: Genes, Genomes, Genetics, 6:3725–3732.

Spencer, H. G., and N. K. Priest. 2016. The evolution of sex-specific dominance in response to sexually antagonistic selection. The American Naturalist, 187:658–666.

Svardal, H., C. Rueffler, and J. Hermisson. 2015. A general condition for adaptive genetic polymorphism in temporally and spatially heterogeneous environemtns. Theoretical Population Biology, 99:76–97.

Tosto, N. M., E. R. Beasley, B. B. Wong, J. E. Mank, and S. P. Flanagan. 2023. The roles of sexual selection and sexual conflict in shaping patterns of genome and transcriptome variation. Nature Ecology & Evolution, 7:981–993.

Wagstaff, B. J., and D. J. Begun. 2005. Molecular population genetics of accessory gland protein genes and testis-expressed genes in *Drosophila mojavensis* and *D. arizonae*. Genetics, 171:1083–1101.

Wilder, S. M., D. Raubenheimer, and S. J. Simpson. 2016. Moving beyond body condition indices as an estimate of fitness in ecological and evolutionary studies. Functional Ecology, 30:108–115.

Wittmann, M. J., A. O. Bergland, M. W. Feldman, P. S. Schmidt, and D. A. Petrov. 2017. Seasonally fluctuating selection can maintain polymorphism at many loci via segregation lift. Proceedings of the National Academy of Sciences, 114:E9932–E9941.

Wong, H. W., and L. Holman. 2023. Pleiotropic fitness effects across sexes and ages in the *Drosophila* genome and transcriptome. Evolution, 77:2642–2655.

Wright, A. E., M. Fumagalli, C. R. Cooney, N. I. Bloch, F. G. Vieira, S. D. Buechel, N. Kolm, and J. E. Mank. 2018. Male-biased gene expression resolves sexual conflict through the evolution of sex-specific genetic architecture. Evolution Letters, 2:52–61.

Wright, S. 1931. Evolution in Mendelian populations. Genetics, 16:97–159.

Wright, S. 1934. Physiological and evolutionary theories of dominance. The American Naturalist, 68:24–53.

Supplementary Information to: Sex-specific Dominance and Its Effects on Allelic Diversity in Sexually Antagonistic Loci

Mattias Siljestam[1*] **and Claus Rueffler**[1†], **Göran Arnqvist**[1†]

[1]Department of Ecology and Genetics, Animal Ecology, Uppsala University, Norbyvägen 18D, 752 36 Uppsala, Sweden
[*]To whom correspondence should be addressed. E-mail: m@siljestam.com
[†]These authors share senior authorship
ORCIDs: Siljestam, https://orcid.org/0000-0002-3720-4926; Rueffler, https://orcid.org/0000-0001-9836-2752; Arnqvist, https://orcid.org/0000-0002-3501-3376

S1. Supplementary figures

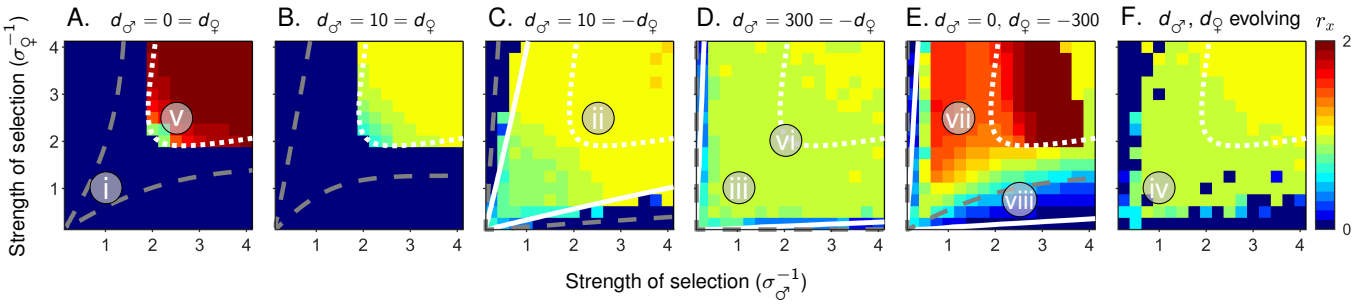

Figure S1. Maximum difference in allelic value between all coexisting alleles at an autosomal locus under sexually antagonistic selection as a function of the strength of selection in the two sexes ($\sigma_♀^{-1}$ and $\sigma_♂^{-1}$) derived from individual-based simulations. Each panel in this figure complements the corresponding panel in Fig. 5 in the main part. Roman numerals are placed at parameter combinations for which a simulated evolutionary tree is shown in the corresponding panel in Figs. 4 and S3.

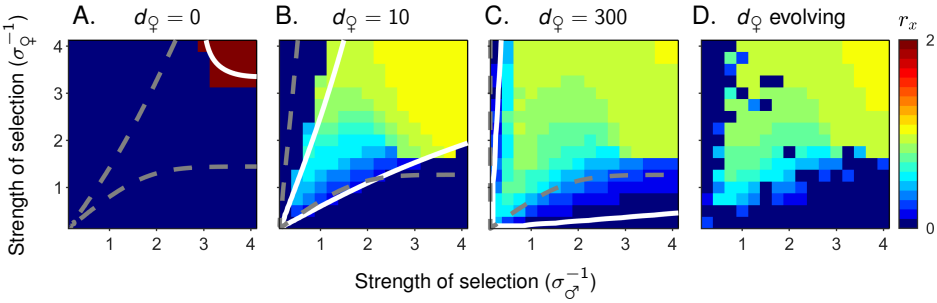

Figure S2. Maximum difference in allelic value between all coexisting alleles at an X-linked locus under sexually antagonistic selection as a function of the strength of selection in the two sexes ($\sigma_♀^{-1}$ and $\sigma_♂^{-1}$) derived from individual-based simulations. Each panel in this figure complements the corresponding panel in Fig. 6 in the main part.

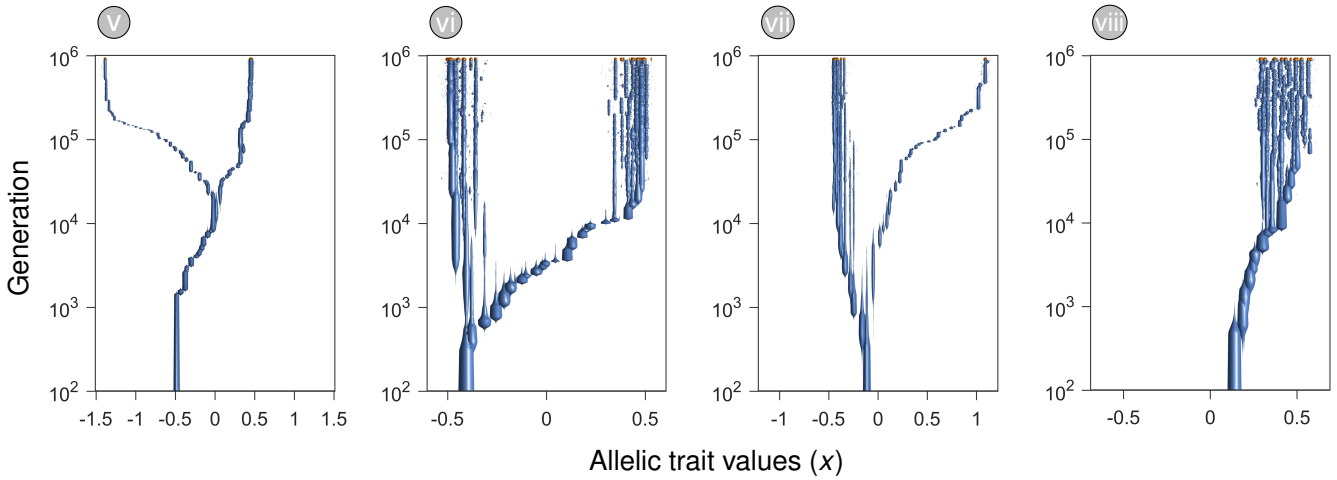

Figure S3. Individual-based simulations showing the evolution of allelic values at an autosomal locus under sexually antagonistic selection. Parameter values for each simulation are given by the location of the Roman numerals in Figure S1. (v) Under additive allelic effects ($d_{♀} = 0 = d_{♂}$) and strong selection ($\sigma_{♀} = 2.5 = \sigma_{♂}$, as in Fig. 1C), we find a BAP with one allele specialized for one sex while the other allele evolves a value overshooting the optimum for the other sex. See text in the main part for further explanations. (vi) Under full adaptive dominance reversal ($d_{♀} = -300$ and $d_{♂} = 300$, as in Fig. 3) and strong selection ($\sigma_{♀} = \sigma_{♂} = 2$), two allelic clusters evolve, each centered around one of the sex-specific optima. Note, that polymorphism emerges far away from the evolutionary branching point at $x^* = 0$. The reason is that under increasingly strong adaptive sex-specific dominance, smaller and smaller allelic differences allow for coexistence due to marginal overdominance. Asymmetric allelic distributions emerge under asymmetric dominance (full dominance in one sex and additivity in the other, as in Fig. 3B) and asymmetric selection. (vii) shows results for $\sigma_{♀}^{-1} = 2.5$ and $\sigma_{♂}^{-1} = 1$ (as in Fig. 1B) and (viii) for $\sigma_{♀} = 0.75, \sigma_{♂} = 2.5$. In (vii), an allelic cluster around one sex-specific optimum cooccurs together with one allele that overshoots the optimum for the other sex. In (viii), we find a PAP that is tightly clustered around one sex-specific optimum. This occurs whenever allelic diversification occurs in a parameter region where the two specialist alleles cannot coexist (below the grey hatched line in Fig. S1E).

S2. Mathematical analysis

We investigate whether selection at a locus subject to sexually antagonistic selection favours a single allele or leads to polymorphism. Our study encompasses both the case of autosomal and X-linked loci. We here address this question through evolutionary invasion analysis using the adaptive dynamics framework (Metz et al., 1992; Geritz et al., 1998; Doebeli, 2011).

S2.1. Survival. In our model, selection acts on a trait that affects survival. Specifically, an individual's survival probability w_k, for sex $k \in \{♀, ♂\}$, is determined by its phenotype z_k. The phenotype z_k is coded by the two alleles x_i and x_j according to

$$z_k(x_i, x_j) = \frac{\delta}{d_k} \ln\left(\frac{e^{d_k x_i} + e^{d_k x_j}}{2}\right). \qquad \text{[S1]}$$

Here, δ denotes the distance between the sex specific optima and d_k the degree and direction of dominance. We call dominance sex-specific if $d_♂ \neq d_♀$. For $d_k \to \infty$, we obtain complete dominance of the allele associated with the larger trait value, resulting in $z_k(x_i, x_j) = \max(x_i, x_j)$. Conversely, $d_k \to -\infty$ results in complete dominance of the allele for the smaller trait value, leading to $z_k(x_i, x_j) = \min(x_i, x_j)$. For a homozygote genotype, Equation S1 results in $z_k(x, x) = x$. In the case of heterozygotes, the phenotype z_k falls between x_i and x_j, and its exact value is determined by the dominance relationship between x_i and x_j. As Equation S1 is not defined for $d = 0$, we replace in this case the right-hand side with its limit for $d \to 0$, namely $\delta(x_i + x_j)/2$. Hence, for $d = 0$ the two alleles act additively. For an X-linked locus, males are hemizygous, possessing only one allele inherited from their mother. For this case we assume that the relationship between allelic value and phenotypic trait is also direct, $z(x) = \delta x$.

Survival probability (or viability) is modelled as a Gaussian function of the difference between an individual's phenotype z and the sex-specific optimal phenotype δ_k,

$$w_k(x_i, x_j) = w_{\max} \exp\left(-\frac{(\delta_k - z_k(x_i, x_j))^2}{2\sigma_k^2}\right). \qquad \text{[S2]}$$

Here, σ_k determines the width of the Gaussian curve for sex k, and $w_{\max}$ denotes the survival reached by an optimal phenotype. For hemizygous males, the viability function simplifies to

$$w_♂(x) = w_{\max} \exp\left(-\frac{(\delta_♂ - z(x))^2}{2\sigma_♂^2}\right), \qquad \text{[S3]}$$

where $z(x) = \delta x$. Note, that $w_{\max}$ is omitted from all subsequent calculations, as it cancels out in both Equation S7 and Equation S8.

Without loss of generality, we define the female and male optima as $\delta_♂ = -\delta/2$ and $\delta_♀ = \delta/2$, respectively, where δ gives the distance between these optima. As a consequence, sex-specific dominance is adaptive if $d_♂ > d_♀$ since under this condition in each sex the allele that has a value closer to the sex-specific optimum has a larger effect on the trait value z.

S2.2. Allele frequency dynamics. Our analysis assumes a large population of fixed size N under Wright-Fisher population dynamics with mutation and selection (Fisher, 1930; Wright, 1931). We denote the allele frequencies among female and males as $p_1, p_2, \ldots, p_n$ and $q_1, q_2, \ldots, q_n$, respectively, in a population with n alleles $x_1, \ldots, x_n$.

Individuals produce, independent of their genotype, a large and equal number of female and male offspring, allowing genotype frequencies among offspring to be deterministically predicted by the allele frequencies of the parents. Mating is random and each offspring is assigned a random mother and father from the parent generation. The expected frequency of offspring with a genotype compris-

ing the alleles x_i and x_j is then given by Hardy-Weinberg proportions, $(p_i q_j + p_j q_i)/2$, before viability selection. Viability selection is sex- and genotype-specific, and the resulting sex-ratio can deviate from 1:1. Viability of an individual carrying the alleles x_i and x_j is determined by the sex-specific survival probability functions $w_{♀}(x_i, x_j)$ for females and $w_{♂}(x_i, x_j)$ for males (see Eq. S2 and Fig. 1 in the main part). For the case of X-linked loci, a hemizygote male, possessing only a single allele x_i, viability is defined by the function $w_{♂}(x_i)$ (see Eq. S3). Finally, N surviving offspring are randomly sampled to represent the adults in the subsequent generation. For our analytical result below, we assume N to be sufficiently large for this to be deterministic, but for the simulations (Figs. 4, 5 and 6), stochasticity is introduced by random multinomial sampling of N surviving offspring, which constitute the adult population of the next generation.

The expected frequencies of an allele x_i in the subsequent generation, collected in the column vector $\boldsymbol{p}'_i$ with entries p'_i and q'_i, are determined by the matrix recursion $\boldsymbol{p}'_i = \mathsf{A}_i \boldsymbol{p}_i$, which we also write as

$$\begin{pmatrix} p'_i \\ q'_i \end{pmatrix} = \begin{pmatrix} a_i & b_i \\ c_i & d_i \end{pmatrix} \begin{pmatrix} p_i \\ q_i \end{pmatrix}. \qquad \text{[S4]}$$

For an autosomal locus, the matrix entries are

$$a_i = \frac{1}{2\bar{w}_{♀}} \sum_j q_j w_{♀}(x_i, x_j), \qquad \text{[S5a]}$$

$$b_i = \frac{1}{2\bar{w}_{♀}} \sum_j p_j w_{♀}(x_j, x_i), \qquad \text{[S5b]}$$

$$c_i = \frac{1}{2\bar{w}_{♂}} \sum_j q_j w_{♂}(x_i, x_j), \qquad \text{[S5c]}$$

$$d_i = \frac{1}{2\bar{w}_{♂}} \sum_j p_j w_{♂}(x_j, x_i), \qquad \text{[S5d]}$$

where $\bar{w}_{♀}$ and $\bar{w}_{♂}$ represent the population mean viability among females and males, respectively.

For an X-linked locus, where males are hemizygous possessing only one allele inherited from their mother, the expected frequency of male offspring carrying allele x_i is directly given by the allele frequency among the adult females, p_i. Consequently, the entries of the matrix A_i for an X-linked locus are

$$a_i = \frac{1}{2\bar{w}_{♀}} \sum_j q_j w_{♀}(x_i, x_j), \qquad \text{[S6a]}$$

$$b_i = \frac{1}{2\bar{w}_{♀}} \sum_j p_j w_{♀}(x_j, x_i), \qquad \text{[S6b]}$$

$$c_i = \frac{w_{♂}(x_i)}{\bar{w}_{♂}}, \qquad \text{[S6c]}$$

$$d_i = 0. \qquad \text{[S6d]}$$

S2.3. Adaptive dynamics.

S2.3.1. Invasion fitness. In our evolutionary invasion analysis, we consider a large resident population monomorphic for allele x, to which we iteratively introduce an initially rare mutant allele $y = x + \epsilon$. As long as the mutant allele remains rare, meaning its frequencies p_y and q_y are negligible, the recursion equation for an autosomal locus (Eqs. S4, and S5) simplifies to

$$\begin{pmatrix} p'_y \\ q'_y \end{pmatrix} = \frac{1}{2} \begin{pmatrix} f & f \\ m_{\mathrm{A}} & m_{\mathrm{A}} \end{pmatrix} \begin{pmatrix} p_y \\ q_y \end{pmatrix}. \qquad \text{[S7]}$$

Similarly, for an X-linked locus, the recursion equation (Eqs. S4 and S6) becomes

$$\begin{pmatrix} p'_y \\ q'_y \end{pmatrix} = \frac{1}{2} \begin{pmatrix} f & f \\ 2m_{\mathrm{X}} & 0 \end{pmatrix} \begin{pmatrix} p_y \\ q_y \end{pmatrix}. \qquad \text{[S8]}$$

Here, the matrix entry $f = w_{♀}(y, x)/w_{♀}(x, x)$ represents the relative survival of a female carrying the mutant allele, and the entries $m_{\mathrm{A}} = w_{♂}(y, x)/w_{♂}(x, x)$ and $m_{\mathrm{X}} = w_{♂}(y)/w_{♂}(x)$ represent the relative survival of male mutants for autosomal and X-linked loci, respectively.

A rare allele y increases in frequency if the dom-

inant eigenvalue $\lambda(y,x)$ of the matrix A on the right-hand side of Equations S7 and S8 is larger than one. Following Metz et al. (1992) and Metz (2008), we refer to $\lambda(y,x)$ as invasion fitness. This eigenvalue is given by

$$\lambda(y,x) = \frac{\mathrm{Tr}(\mathsf{A}) + \sqrt{\mathrm{Tr}(\mathsf{A})^2 - 4\mathrm{Det}(\mathsf{A})}}{2}. \qquad \text{[S9]}$$

In the autosomal case, we obtain

$$\begin{aligned}\lambda_i &= \frac{f + m_{\mathrm{A}} + \sqrt{(f+m_{\mathrm{A}})^2 - 0}}{4} \\ &= \frac{f + m_{\mathrm{A}}}{2} \\ &= \frac{1}{2}\left(\frac{w_{♀}(y,x)}{w_{♀}(x,x)} + \frac{w_{♂}(y,x)}{w_{♂}(x,x)}\right), \qquad \text{[S10]}\end{aligned}$$

which we recognize as the Shaw-Mohler equation (Shaw and Mohler, 1953).

For an X-linked locus, we obtain

$$\lambda(y,x) = \frac{f + \sqrt{f(f+8m_{\mathrm{X}})}}{4}. \qquad \text{[S11]}$$

In this case, invasion criterion $\lambda(y,x) > 1$ simplifies to

$$\begin{aligned} & \lambda(y,x) > 1 \\ \iff \quad & f + \sqrt{f^2 + 8fm_{\mathrm{X}}} > 4 \\ \iff \quad & f^2 + 8fm_{\mathrm{X}} > 16 - 8f + f^2 \\ \iff \quad & \frac{f + fm_{\mathrm{X}}}{2} > 1. \qquad \text{[S12]}\end{aligned}$$

We denote the fitness proxy given by the left-hand side in the last inequality as $\tilde{\lambda}(y,x)$. Using the definitions for f and m_{X}, we obtain

$$\begin{aligned}\tilde{\lambda}(y,x) &= \frac{f + fm_{\mathrm{X}}}{2} \\ &= \frac{1}{2}\frac{w_{♀}(y,x)}{w_{♀}(x,x)}\left(1 + \frac{w_{♂}(y)}{w_{♂}(x)}\right). \qquad \text{[S13]}\end{aligned}$$

Since $\tilde{\lambda}(y,x) \lesseqgtr 1 \iff \lambda(y,x) \lesseqgtr 1$, we can use $\tilde{\lambda}(y,x)$ for all further calculations concerning X-linked loci.

S2.4. Singular points. Given that mutations have small effect ($y = x + \epsilon$ with ϵ small), the direction of evolutionary change is given by the selection gradient

$$D(x) = \left.\frac{\partial \lambda(y,x)}{\partial y}\right|_{y=x} \qquad \text{[S14]}$$

(Geritz et al., 1998). If mutations occur infrequently, a mutant allele y either goes extinct or reaches an equilibrium frequency before the next mutant appears. Furthermore, if $D(x) \neq 0$ and still assuming small mutational effects, then invasion of y implies extinction of x (Dercole and Rinaldi, 2008; Priklopil and Lehmann, 2020). Iterating this process results in a trait substitution sequence of allelic values, giving the long-term evolutionary dynamics (Champagnat et al., 2006).

To determine the selection gradient for an autosomal locus, we substitute Equation S10 into Equation S14, resulting in

$$D(x) = \frac{1}{2}\left.\left(\frac{\partial}{\partial y}\frac{w_{♀}(y,x)}{w_{♀}(x,x)} + \frac{\partial}{\partial y}\frac{w_{♂}(y,x)}{w_{♂}(x,x)}\right)\right|_{y=x}. \qquad \text{[S15]}$$

Utilizing the derivatives of the survival function provided in section S2.6 below, and substituting Equation S32 into Equation S15, we derive the selection gradient for an autosomal locus as

$$\begin{aligned}D(x) &= \frac{\delta^2}{4}\left(\frac{1/2 - x}{\sigma^2_{♂}} - \frac{1/2 + x}{\sigma^2_{♀}}\right) \\ &= \frac{\delta^2}{4}\left(\frac{1}{2}(\sigma^2_{♀} - \sigma^2_{♂}) - x(\sigma^2_{♀} + \sigma^2_{♂})\right). \qquad \text{[S16]}\end{aligned}$$

For an X-linked locus, we obtain

$$\begin{aligned}\tilde{D}(x) &= \left.\frac{\partial \tilde{\lambda}(y,x)}{\partial y}\right|_{y=x} \\ &= \left.\frac{\partial}{\partial y}\frac{w_{♀}(y,x)}{w_{♀}(x,x)}\right|_{y=x} + \frac{1}{2}\left.\frac{\partial}{\partial y}\frac{w_{♂}(y)}{w_{♂}(x)}\right|_{y=x}. \qquad \text{[S17]}\end{aligned}$$

Substituting Equations S32 and S34 into Equation S17, we see that the selection gradient for the X-linked locus is equal to two times the selection gradient for the autosomal case,

$$\tilde{D}(x) = 2D(x). \qquad \text{[S18]}$$

The evolutionary dynamics come to a halt once an allelic value x^* is reached where the selection gradient equals zero, $D(x^*) = 0$ or $\tilde{D}(x^*) = 0$, respectively. We refer to such allelic values as singular allelic values. Thus, we find a unique singular allelic value x^*, which, due to Equation S18, is the same for autosomal and X-linked loci. It is given by

$$x^* = \frac{1}{2}\frac{\sigma_{♀}^2 - \sigma_{♂}^2}{\sigma_{♀}^2 + \sigma_{♂}^2} \qquad \text{[S19]}$$

Under symmetric selection strength ($\sigma_{♀}^{-2} = \sigma_{♂}^{-2}$), the singular allelic value simplifies to $x^* = 0$, representing the midpoint between the two sex-specific optima.

We note that the selection gradient $D(x)$ for the autosomal case and $\tilde{D}(x)$ for the X-linked case can be expressed as

$$D(x) = \tilde{D}(x)/2 = g'(x), \qquad \text{[S20]}$$

where

$$g(x) = \frac{1}{2}\ln\left(\sqrt{w_{♀}(x,x)w_{♂}(x,x)}\right). \qquad \text{[S21]}$$

Thus, selection acts to increase geometric mean survival averaged, both for autosomal (Charnov, 1982; Leimar, 2001) and X-linked loci.

S2.5. Classification of the singular point. Singular allelic values x^* can be attractors or repellers of trait substitution sequences (Geritz et al., 1998; Doebeli, 2011). Values x^* that are attractors are referred to as convergence stable. Furthermore, singular allelic values x^* can be invadable or uninvadable by nearby mutants. Values x^* that are both convergence stable and uninvadable are evolutionary endpoints (also called continuously stable strategies), while values x^* that are convergence stable and invadable are evolutionary branching points where adaptive allelic polymorphism can emerge.

Since our model has a unique singular point x^* in a one-dimensional trait space ($x \in \mathbb{R}$), x^* is either convergence stable or, if it is not convergence stable, the evolutionary dynamics approach $-\infty$ or $+\infty$. Since in the latter case, survival of both sexes approaches zero, we can conclude that x^* is convergence stable. The same conclusion can be reached by noting that

$$g''(x) = -\frac{\delta^2}{4}\left(\frac{1}{\sigma_{♀}^2} + \frac{1}{\sigma_{♂}^2}\right) < 0. \qquad \text{[S22]}$$

By determining whether x^* is invadable, we can distinguish evolutionary endpoints from evolutionary branching points.

S2.5.1. Invadability. The evolutionary singular allele x^* can be invadable or uninvadable, which is determined by the sign of the second-order partial derivative with respect to the mutant trait y,

$$\left.\frac{\partial^2\lambda(y,x)}{\partial y^2}\right|_{y=x=x^*}. \qquad \text{[S23]}$$

If this derivative is positive, then x^* is a local fitness minimum and can be invaded by nearby mutants while a negative second derivative indicates a local fitness maximum and x^* cannot be invaded by nearby mutants. Singular allelic values that are both convergence stable and invadable are evolutionary brancing points, where polymorphism can emerge (Geritz et al., 1998; Doebeli, 2011). To simplify notation, we assume from now on that all derivatives are evaluated at $y = x = x^*$.

Autosomal locus. For an autosomal locus, we obtain

$$\begin{aligned}\frac{\partial^2\lambda(y,x)}{\partial y^2} &= \frac{1}{2}\left(\frac{\frac{\partial^2}{\partial y^2}w_{♀}(y,x)}{w_{♀}(x,x)} + \frac{\frac{\partial^2}{\partial y^2}w_{♂}(y,x)}{w_{♂}(x,x)}\right)\\ &= \sum_{k\in\{♀,♂\}}\frac{(\delta_k - x^*)^2 + (\delta_k - x^*)d_k\sigma_k^2 - \sigma_k^2}{8\sigma_k^4}\\ &= \frac{\delta^2}{4} + (d_{♂} - d_{♀})\frac{(\sigma_{♀}^2 + \sigma_{♂}^2)}{8} - \frac{(\sigma_{♀}^2 + \sigma_{♂}^2)^3}{8\sigma_{♀}^2\sigma_{♂}^2}.\end{aligned}$$

The second equality is obtained by using the second-order partial derivative of w_k with respect to y, as given in Equation S33, and the last step follows from using the expression for x^* as given by Equation S19.

In summary, the condition for evolutionary branching (see Condition 1 in the main part) is given by

$$\left.\frac{\partial^2\lambda(y,x)}{\partial y^2}\right|_{y=x=x^*} > 0 \iff$$

$$\frac{\delta^2}{4} + (d_{♂} - d_{♀})\frac{(\sigma_{♀}^2 + \sigma_{♂}^2)}{8} > \frac{(\sigma_{♀}^2 + \sigma_{♂}^2)^3}{8\sigma_{♀}^2\sigma_{♂}^2}. \quad \text{[S24]}$$

Under symmetry ($\sigma_{♀}^2 = \sigma^2 = \sigma_{♂}^2$), condition S24 can be rewritten as (Condition 2 in the main part)

$$\frac{\delta^2}{4 - (d_{♂} - d_{♀})} > \sigma^2. \quad \text{[S25]}$$

Under symmetry and in the absence of sex-specific dominance, condition S25 simplifies further to $\delta^2/4 > \sigma^2$.

X-linked locus. For an X-linked locus, an analogous calculation results in

$$\frac{\delta^2}{4} - d_{♀}\frac{(\sigma_{♀}^2 + \sigma_{♂}^2)}{4} > \frac{(\sigma_{♀}^2 + \sigma_{♂}^2)^2(2\sigma_{♀}^2 + \sigma_{♂}^2)}{4\sigma_{♀}^2\sigma_{♂}^2} \quad \text{[S26]}$$

as condition for evolutionary branching. The terms in this condition are analogous to the corresponding terms in condition S24. The difference is that the second term on the left-hand side depends only on $d_{♀}$. Dominance facilitates evolutionary diversification if it is adaptive ($d_{♀} < 0$) and hinders diversification otherwise. The right-hand side of the inequality, capturing the effect of selection strength that is independent of dominance, is slightly different, and under symmetry ($\sigma_{♀}^2 = \sigma = \sigma_{♂}^2$) it simplifies to $3\sigma^2$. Under this symmetry, inequality S26 simplifies to

$$\frac{\delta^2}{2(6 - d_{♀})} > \sigma^2. \quad \text{[S27]}$$

In the absence of dominance ($d_{♀} = 0$), this conditions further simplifies to $\delta^2/4 > 3\sigma^2$, indicating that the condition for evolutionary diversification at an evolutionary branching point is significantly more stringent at an X-linked locus compared to an autosomal locus.

S2.6. Derivatives of the phenotype and survival functions.

In this section, we present derivatives for the phenotypic trait function z_k (Eq. S1) and the viability functions w_k (Eqs. S2 and S3), used in the calculations detailed above.

S2.6.1. Derivatives of the phenotype function.

The partial derivative of the phenotype function $z_k(y,x)$ with the respect to the mutant allele y equals

$$\begin{aligned}\frac{\partial z_k(y,x)}{\partial y} &= \frac{1}{d_k}\frac{\partial}{\partial y}\ln\left(\frac{e^{d_k y} + e^{d_k x}}{2}\right)\\ &= \frac{e^{d_k y}}{e^{d_k y} + e^{d_k x}}. \quad \text{[S28]}\end{aligned}$$

When evaluated at $y = x$, Equation S28 simplifies to

$$\left.\frac{\partial z_k(y,x)}{\partial y}\right|_{y=x} = \frac{1}{2}. \quad \text{[S29]}$$

The second partial derivative of $z_k(y,x)$ with respect to y, evaluated at $y=x$, equals

$$\begin{aligned}\frac{\partial^2 z_k(y,x)}{\partial y^2}\bigg|_{y=x} &= \frac{\partial}{\partial y}\left(\frac{e^{d_k y}}{e^{d_k y}+e^{d_k x}}\right)\bigg|_{y=x}\\ &= d_k\left(\frac{e^{d_k y}e^{d_k x}}{(e^{d_k y}+e^{d_k x})^2}\right)\bigg|_{y=x}\\ &= \frac{d_k}{4}. \qquad \text{[S30]}\end{aligned}$$

S2.6.2. Derivatives of the survival functions. The partial derivative of the survival function $w_k(y,x)$ with respect to y equals

$$\begin{aligned}\frac{\partial w_k(y,x)}{\partial y} &= \frac{\partial}{\partial y}\exp\left(-\frac{(\delta_k - z_k(y,x))^2}{2\sigma_k^2}\right),\\ &= w_k(y,x)\frac{\delta_k - z_k(y,x)}{\sigma_k^2}\frac{\partial z_k(y,x)}{\partial y}, \qquad \text{[S31]}\end{aligned}$$

which, when evaluated at $y=x$, becomes

$$\begin{aligned}\frac{\partial w_k(y,x)}{\partial y}\bigg|_{y=x} &= w_k(x,x)\frac{\delta_k - x}{\sigma_k^2}\frac{\partial z_k(y,x)}{\partial y}\bigg|_{y=x}\\ &= w_k(x,x)\frac{\delta_k - x}{2\sigma_k^2}, \qquad \text{[S32]}\end{aligned}$$

where we use that $z_k(x,x)=\delta x$ and Equation S29.

The second partial derivative of $w_k(y,x)$ with respect to y, evaluated at $y=x$, equals

$$\begin{aligned}&\frac{\partial^2 w_k(y,x)}{\partial y^2}\bigg|_{y=x} = \frac{1}{\sigma_k^2}\frac{\partial}{\partial y}\left(w_k(y,x)\left(\delta_k - z_k(y,x)\right)\frac{\partial z_k(y,x)}{\partial y}\right)\bigg|_{y=x}\\ &= \frac{1}{2\sigma_k^2}\left(\frac{\partial w_k(y,x)}{\partial y}\bigg|_{y=x}(\delta_k - x) - \frac{1}{2}w_k(x,x) + \frac{d_k}{2}w_k(x,x)(\delta_k - x)\right)\\ &= w_k(x,x)\frac{(\delta_k - x)^2 + (\delta_k - x)d_k\sigma_k^2 - \sigma_k^2}{4\sigma_k^4}. \qquad \text{[S33]}\end{aligned}$$

For a hemizygote, the derivative of the survival function $w_{♂}(y)$ with respect to y is

$$\frac{\mathrm{d}w_{♂}(y)}{\mathrm{d}y} = w_{♂}(y)\frac{\delta_{♂} - y}{\sigma_{♂}^2} \qquad \text{[S34]}$$

The second derivative of $w_{♂}(y)$ equals

$$\begin{aligned}\frac{\partial^2 w_{♂}(y)}{\partial y^2} &= \frac{1}{\sigma_{♂}^2}\frac{\partial}{\partial y}\left(w_{♂}(y)(\delta_{♂} - y)\right)\\ &= \frac{1}{\sigma_{♂}^2}\left(\frac{\partial w_{♂}(y)}{\partial y}(\delta_{♂} - y) - w_{♂}(y)\right)\\ &= \frac{1}{\sigma_{♂}^2}\left(w_{♂}(y)\frac{(\delta_{♂} - y)^2}{\sigma_{♂}^2} - w_{♂}(y)\right)\\ &= w_{♂}(y)\frac{(\delta_{♂} - y)^2 - \sigma_{♂}^2}{\sigma_{♂}^4}. \qquad \text{[S35]}\end{aligned}$$

S3. Population genomic data

S3.1. Signals of polyallelic polymorphism in PoolSeq data. The pool-seq data analysed in this contribution derives from Sayadi et al. (2019) (ENA accession PRJEB30475, NCBI accession PRJNA503561) and we refer to that source for detailed methodological information. Pool-seq data contains large amounts of short-read data from multiple individuals sequenced as a pool and is widely used to infer SNP frequencies in populations (e.g., Schlötterer et al., 2014). However, because data is not phased, it is difficult to unambiguously distinguish bi- from polyallelic polymorphism using pool-seq data. In order to do so, we used a simple inferential logic designed to provide a comprehensive signal representing how consistent read-count data is with there being only two segregating alleles (i.e., biallelic polymorphism) in a given locus. We used the $\log P$ from a chi-squared test of the null hypothesis that the read count distribution between the minor and the major base is the same across all SNPs within a gene, as is expected if only two alleles are present in a given population (see Figure S4). The more negative $\log P$ is for a given gene, thus, the less consistent data is with biallelic polymorphism and the more strongly it suggests polyallelic polymorphism.

The pipeline for read-trimming, read-mapping and SNP-calling was very stringent, to avoid false SNPs, mis-mapping and ambiguously mapped reads (Sayadi et al., 2019). Here, we included only genes with two or more well-supported SNPs. Yet, our inferential logic is certainly not free from potential problems, deriving from gene-specific mapping errors, unequal coverage and other unknown complications. However, given the fact that the data is based on a high-quality genome assembly, stringent filtering of read-quality and strict parameters during mapping to avoid falsely mapped reads (Sayadi et al., 2019), the metric used here ($\log P$) should thus carry a true signal of polyallelic polymorphism when averaged across many genes.

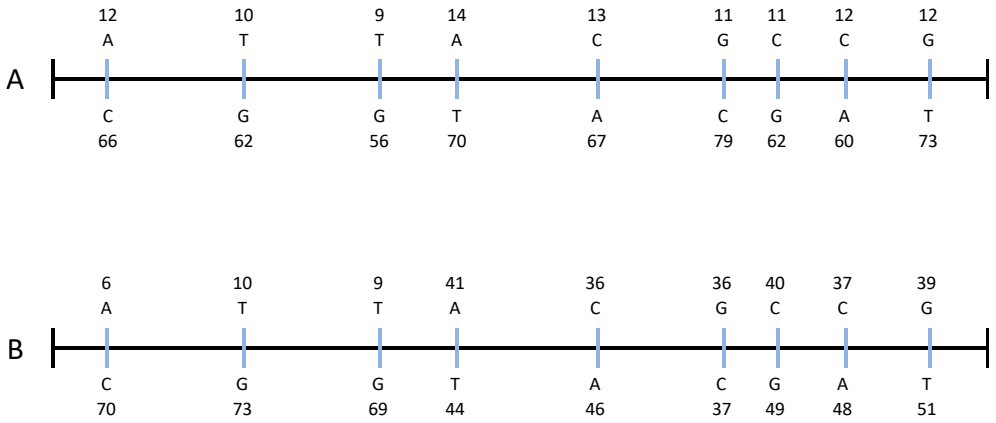

Figure S4. Two hypothetical cases of read-count distributions over a gene with 9 SNPs (blue bars), the upper representing the minor base count and the lower the major base count, illustrating how read-count distributions was used to infer how consistent the data is with two alleles being present among reads from a sequenced pool of individuals. In **A**, the distribution of counts is similar across SNPs which is highly consistent with two segregating alleles with a minor allele (A-T-T-A-C-G-C-C-G) occurring at a frequency of about p = 0.15 ($\chi^2_8 = 1.18, P = 0.997$). In **B**, the distribution of counts is more variable and is highly inconsistent with two segregating alleles ($\chi^2_8 = 88.64, P = 8.77 \times 10^{-16}$). In this particular case, the data is consistent with, for example, an allele A-T-T-A-C-G-C-C-G occuring at about $p = 0.1$, an allele C-G-G-A-C-G-C-C-G at about $p = 0.35$ and an allele C-G-G-T-A-C-G-A-T at about $p = 0.55$.

S3.2. Functional enrichment analysis.

Table S1. Functional enrichment of 64 genes showing a standardized $\log P < -5$ in any of the three populations, against a universe of all polymorphic genes.

	GOCCID	P-value	OddsRatio	ExpCount	Count	Size	Term
1	GO:0045263	0.007822652	254.16667	0.007838014	1	4	proton-transporting ATP synthase complex coupling factor F(o)
2	GO:0045259	0.015604402	108.64286	0.015676029	1	8	proton-transporting ATP synthase complex
3	GO:0033177	0.019479972	84.38889	0.019595036	1	10	proton-transporting two-sector ATPase complex proton-transporting domain
4	GO:0044425	0.03427625	Inf	0.975832789	3	498	membrane part
5	GO:0016469	0.042519966	35.88095	0.043109079	1	22	proton-transporting two-sector ATPase complex

	GOBPID	P-value	OddsRatio	ExpCount	Count	Size	Term
1	GO:0005978	0.008313086	205	0.008333333	1	3	glycogen biosynthetic process
2	GO:0009250	0.008313086	205	0.008333333	1	3	glucan biosynthetic process
3	GO:0044042	0.011070644	136.619048	0.011111111	1	4	glucan metabolic process
4	GO:0005977	0.011070644	136.619048	0.011111111	1	4	glycogen metabolic process
5	GO:0006112	0.011070644	136.619048	0.011111111	1	4	energy reserve metabolic process
6	GO:0006073	0.011070644	136.619048	0.011111111	1	4	cellular glucan metabolic process
7	GO:0033692	0.013821491	102.428571	0.013888889	1	5	cellular polysaccharide biosynthetic process
8	GO:0000271	0.013821491	102.428571	0.013888889	1	5	polysaccharide biosynthetic process
9	GO:0044264	0.01656564	81.914286	0.016666667	1	6	cellular polysaccharide metabolic process
10	GO:0009987	0.021743002	Inf	4.961111111	8	1786	cellular process
11	GO:0034637	0.0220339	58.469388	0.022222222	1	8	cellular carbohydrate biosynthetic process
12	GO:0005976	0.0220339	58.469388	0.022222222	1	8	polysaccharide metabolic process
13	GO:0044763	0.02351814	5.71183	2.763888889	6	995	single-organism cellular process
14	GO:0015985	0.02475804	51.142857	0.025	1	9	energy coupled proton transport down electrochemical gradient
15	GO:0015986	0.02475804	51.142857	0.025	1	9	ATP synthesis coupled proton transport
16	GO:0006754	0.02475804	51.142857	0.025	1	9	ATP biosynthetic process
17	GO:0015980	0.030186407	40.885714	0.030555556	1	11	energy derivation by oxidation of organic compounds
18	GO:0044249	0.03111107	4.995825	1.341666667	4	483	cellular biosynthetic process
19	GO:1901576	0.032445586	4.921649	1.358333333	4	489	organic substance biosynthetic process
20	GO:0016051	0.032890662	37.155844	0.033333333	1	12	carbohydrate biosynthetic process
21	GO:0009168	0.032890662	37.155844	0.033333333	1	12	purine ribonucleoside monophosphate biosynthetic process
22	GO:0009127	0.032890662	37.155844	0.033333333	1	12	purine nucleoside monophosphate biosynthetic process
23	GO:0006259	0.035408622	8.449541	0.308333333	2	111	DNA metabolic process
24	GO:0009142	0.035588317	34.047619	0.036111111	1	13	nucleoside triphosphate biosynthetic process
25	GO:0009145	0.035588317	34.047619	0.036111111	1	13	purine nucleoside triphosphate biosynthetic process
26	GO:0009201	0.035588317	34.047619	0.036111111	1	13	ribonucleoside triphosphate biosynthetic process
27	GO:0009206	0.035588317	34.047619	0.036111111	1	13	purine ribonucleoside triphosphate biosynthetic process
28	GO:0044711	0.036001873	8.369697	0.311111111	2	112	single-organism biosynthetic process
29	GO:0009156	0.038279386	31.417582	0.038888889	1	14	ribonucleoside monophosphate biosynthetic process
30	GO:0009058	0.039669764	4.576699	1.441666667	4	519	biosynthetic process
31	GO:0009124	0.040963882	29.163265	0.041666667	1	15	nucleoside monophosphate biosynthetic process
32	GO:0006139	0.041227019	4.512476	1.458333333	4	525	nucleobase-containing compound metabolic process
33	GO:0007165	0.04471132	5.068421	0.852777778	3	307	signal transduction
34	GO:0006725	0.045009297	4.368224	1.497222222	4	539	cellular aromatic compound metabolic process
35	GO:0044700	0.045849014	5.013029	0.861111111	3	310	single organism signaling
36	GO:0023052	0.045849014	5.013029	0.861111111	3	310	signaling
37	GO:0007154	0.046231702	4.994805	0.863888889	3	311	cell communication
38	GO:0046129	0.04631321	25.5	0.047222222	1	17	purine ribonucleoside biosynthetic process
39	GO:0042451	0.04631321	25.5	0.047222222	1	17	purine nucleoside biosynthetic process
40	GO:0046483	0.046411008	4.318519	1.511111111	4	544	heterocycle metabolic process
41	GO:1901360	0.047839722	4.269725	1.525	4	549	organic cyclic compound metabolic process
42	GO:0006091	0.04897807	23.991597	0.05	1	18	generation of precursor metabolites and energy

	GOMFID	P-value	OddsRatio	ExpCount	Count	Size	Term
1	GO:0003676	0.000162235	4.878353	3.9312135	12	699	nucleic acid binding
2	GO:0004373	0.011217687	183.84	0.01124811	1	2	glycogen (starch) synthase activity
3	GO:0008144	0.011217687	183.84	0.01124811	1	2	drug binding
4	GO:0017025	0.011217687	183.84	0.01124811	1	2	TBP-class protein binding
5	GO:0046527	0.011217687	183.84	0.01124811	1	2	glucosyltransferase activity
6	GO:0008408	0.03329117	36.736	0.03374432	1	6	3'-5' exonuclease activity